Supplement of Biogeosciences, 22, 4903–4922, 2025
https://doi.org/10.5194/bg-22-4903-2025-supplement

Biogeosciences Open Access EGU

Supplement of

European tree cover during the Holocene reconstructed from pollen records

Luke Sweeney et al.

Correspondence to: Luke Sweeney (l.sweeney@pgr.reading.ac.uk)

Supplementary information

Contents

This supplement contains the following sections:

Section S1: Sources for SMPDSv2 data

Table S1 provides the metadata source for the SMPDsv2 data, together with the number of entities/records and citations for each source.

Table S1: List of SMPDSv2 data sources and references

Source (metadata table)	Number of entities	Publications
AMSS	38	Jolly et al., 1996; Julier et al., 2019, 2018; Lebamba et al., 2009
APD	90	Vincens et al., 2007
Australasian pollen	1540	Adeleye et al., 2021b, 2021a; Beck et al., 2017; Field et al., 2018; Fletcher et al., 2014; Herbert and Harrison, 2016; Luly, 1993; Luly et al., 1986; Mariani et al., 2017; McWethy et al., 2010, 2014; Pickett et al., 2004; Prebble et al., 2019
BIOME6000 Japan	94	Takahara et al., 2000
Blyakharchuk	144	Author: Tatiana A. Blyakharchuk
Bush et al., 2021	636	Bush et al., 2021
CMPD	4208	Chen et al., 2021
Dugerdil et al., 2021	48	Dugerdil et al., 2021
EMBSeCBIO	149	Harrison et al., 2021
EMPDv2	3508	Davis et al., 2020
Gaillard et al., 1992	124	Gaillard et al., 1992
Harrison et al., 2022b	3	Harrison et al., 2022b
Herzschuh et al., 2019	595	Herzschuh et al., 2019
IBERIA	243	Harrison et al., 2022a
Neotoma	6702	Williams et al., 2018
Phelps et al., 2020	106	Phelps et al., 2020
SMPDSv1	6345	Harrison, 2019
Southern Hemisphere pollen	76	Black, 2007; Dodson, 1978; Dodson and Intoh, 1999; Haberle, 1993, 1996; Hope, 2009; Hope et al., 1998, 1999; Macphail, 1975, 1979, 1980; Macphail and McQueen, 1983; Macphail and Mildenhall, 1980; Norton et al., 1986; Prebble et al., 2010; Shulmeister et al., 2003

Section S2: Species categorisation

Table S2 lists the higher level groupings of taxa considered native to Europe and included within the Total Terrestrial Pollen Sum. Species are grouped into trees, shrubs and woody vines, and herbaceous pollen (herbs, grasses etc.). Tree species are sub-divided into broadleaf and needleleaf, and into wind pollinated, biotic pollination or dual wind/biotic pollination. Assigning species into pollination method categories is challenging, especially for pollen only identified at the family level. For the most part, species were assigned into wind pollinated, biotic pollination and dual wind and biotic pollination following the categorisation by Tong et al. (2023)., supplemented by information from Kling and Ackerley (2021). For *Buxus*, *Castanea* and *Fraxinus*, we assigned these species as wind pollinated, as although they are biotically pollinated, they are for the most part pollinated by wind. Similarly, we categorised *Cornus*, *Laburnum*, *Laurus*, *Salix* and *Vitex* as primarily biotically pollinated, despite some wind pollination occurring for these species. This data in csv form is downloadable from https://doi.org/10.5281/zenodo.15283096

Table S2: Classification of taxa included within the Total Terrestrial Pollen Sum

Tree/Shrub/Non-arboreal		**Taxa grouping**
Tree	Broadleaf	*Acer*, *Aesculus*, *Alnus*, *Alnus* subg. *Alnobetula*, Anacardiaceae, *Arbutus*, Arecaceae, *Betula*, *Betula chamaebetula*, *Buxus*, *Carpinus*, *Carpinus betulus*, *Carpinus orientalis/Ostrya*, *Castanea*, *Celtis*, *Ceratonia*, *Cercis*, *Citrus*, Clusiaceae, Cornaceae, *Cornus*, *Corylus*, Elaeagnaceae, *Elaeagnus*, Fabaceae, *Fagus*, *Ficus*, *Fontanesia*, *Fraxinus*, *Ilex*, Juglandaceae, *Juglans*, *Laburnum*, *Laurus*, *Malus*, *Malus/Pyrus*, Moraceae, Moraceae/Urticaceae, Myricaceae, Myrtaceae, *Olea*, Oleaceae, *Pistacia*, *Platanus*, *Populus*, *Prunus*, *Pyrus*, *Quercus*, *Quercus* deciduous, *Quercus* evergreen, *Salix*, Sapindaceae, *Sorbus*, Staphyleaceae, *Syringa*, *Tamarix*, Thymelaeaceae, *Tilia*, Ulmaceae, *Ulmus*, *Ulmus/Zelkova*, Verbenaceae, Viburnaceae, *Viburnum*, *Vitex*
	Needleleaf	*Abies*, *Cedrus*, Cupressaceae, Cupressaceae/Taxaceae, *Larix*, *Larix/Pseudotsuga*, *Picea*, *Pinus*, *Pinus* (diploxylon), *Pinus* (haploxylon), *Taxus*
Tree	Wind pollinated	*Abies, Acer, Alnus, Alnus subg. Alnobetula, Betula, Betula chamaebetula, Carpinus, Carpinus betulus, Carpinus orientalis/Ostrya, Cedrus, Celtis, Corylus,* Cupressaceae*, Fagus,* Juglandaceae*, Juglans, Larix, Larix/Pseudotsuga, Olea, Picea, Pinus, Pinus (diploxylon), Pinus (haploxylon), Pistacia, Platanus, Populus, Quercus, Quercus deciduous, Quercus evergreen, Taxus, Ulmus, Ulmus/Zelkova, Pinus (diploxylon), Pinus (haploxylon),* Ulmaceae*,* Myricaceae*,* Cupressaceae/Taxaceae
	Biotic pollination	*Aesculus, Arbutus, Cercis, Citrus, Clusiaceae, Elaeagnus, Ficus, Fontanesia, Ilex, Malus, Malus/Pyrus, Prunus, Pyrus, Sorbus,* Staphyleaceae*, Syringa, Tamarix, Tilia,* Viburnaceae*, Viburnum*
	Dual wind and biotic pollination	Anacardiaceae*,* Arecaceae*, Buxus, Castanea, Ceratonia,* Cornaceae*, Cornus,* Elaeagnaceae*,* Fabaceae*, Fraxinus, Laburnum, Laurus,* Moraceae*,* Moraceae/Urticaceae*,* Myrtaceae*,* Oleaceae*, Salix,* Sapindaceae*,* Thymelaeaceae*,* Verbenaceae*, Vitex*
Shrub and woody vine		Acanthaceae, *Alhagi*, *Andromeda*, Apiaceae, Araliaceae, Aristolochiaceae, *Artemisia*, Asparagaceae, *Astragalus*, Berberidaceae, *Berberis*, *Buddleia*, *Calicotome*, *Calluna*, Capparaceae, Caprifoliaceae, *Cassiope*, *Chamaedaphne*, Cistaceae, *Cistus*, *Citrullus*, *Clematis*, *Clethra*, *Colutea*, Convolvulaceae, *Coriaria*, *Cotinus*, *Cotoneaster*, *Crataegus*, Cucurbitaceae, *Daphne*, *Diapensia*, *Dioscorea*, Dioscoreaceae, *Dryas*, *Empetrum*, *Ephedra*, Ephedraceae, *Erica*, Ericaceae, *Euonymus*, *Flueggea*, *Forsythia*, *Frangula*, Frankeniaceae, Genisteae, *Halimium*, *Hedera*, *Helianthemum*, *Hippophae*, *Kalmia*, *Lavandula*, *Ledum*, *Ligustrum*, *Linnaea*, *Lonicera*, Malvaceae, *Moltkia*, Montiaceae, *Myrica*, *Myricaria*, *Nerium*, Nitrariaceae, *Ononis*, *Osmanthus*, *Paeonia*, *Paliurus*, *Periploca*, *Phillyrea*, *Phlomis*, *Potentilla*, Rhamnaceae, *Rhamnus*, *Rhododendron*, *Rhus*, *Ribes*, Rosaceae, *Rubus*, *Ruscus*, *Salvia*, *Sambucus*, Sapotaceae, *Smilax*, *Styrax*, *Suaeda*, *Vaccinium*, *Ziziphus*
Herbaceous		*Aconitum*, *Actaea*, Aizoaceae, Amaranthaceae, Amaryllidaceae, Apocynaceae, *Aquilegia*, Araceae, Asphodelaceae, Asteraceae, Asteraceae (Liguliflorae), Asteroideae, Balsaminaceae, Boraginaceae, Brassicaceae, Campanulaceae, Cannabaceae, Carduoideae, Caryophyllaceae,

	Celastraceae, *Chimaphila*, Cichorioideae, Colchicaceae, Commelinaceae, *Consolida*, Crassulaceae, Cyperaceae, *Datisca*, *Delphinium*, Eriocaulaceae, Euphorbiaceae, Fabaceae (herbs), Gentianaceae, Geraniaceae, *Helleborus*, Hypericaceae, *Impatiens*, Iridaceae, *Koenigia*, Lamiaceae, Liliaceae, Linaceae, Linderniaceae, *Linum*, *Lysimachia*, Lythraceae, *Malva*, Melanthiaceae, *Mercurialis*, Nartheciaceae, *Nigella*, Onagraceae, Orchidaceae, Oxalidaceae, *Oxyria/Rumex*, Papaveraceae, Penthoraceae, Phyllanthaceae, Plantaginaceae, Plumbaginaceae, Poaceae, Polemoniaceae, Polygalaceae, Polygonaceae, *Polygonum*, Polypodiales, Portulacaceae, Primulaceae, Ranunculaceae, *Ranunculus*, Resedaceae, Rubiaceae, Rutaceae, *Sanguisorba*, Santalaceae, Saxifragaceae, Scrophulariaceae, Solanaceae, *Teucrium*, *Thalictrum*, *Tofieldia*, *Trollius*, Urticaceae, Violaceae, Zygophyllaceae

Section S3: Coefficients and model fit including %wind pollination or %Pinus

Including the %wind pollinated within the regression model instead of %needleleaf, also with a second-degree polynomial, led to a reduction in the model pseudo (Cox-Snell) R^2 to 0.56 (compared to 0.60). LOOCV MAE increased to 0.12 (from 0.11), RMSE increased to 0.15 from 0.14 and the squared correlation (R^2) of the predictions to the observations was reduced to 0.57 (from 0.63). The model coefficients are shown in Table S3; although the coefficient values change compared to the model with %needleleaf, the directions of the coefficients remain the same. The slight reduction in model fit reflects the fact that %needleleaf also partially accounts for differences in pollen productivity, as well as differences in pollen transport. As well as selecting the tree species classified as wind pollinated only, we also investigated the model fit when including both those species classified as wind pollinated and those species classified as both wind and biotically pollinated. In this case the model fit was similarly worse than using %needleleaf, with the pseudo (Cox-Snell) R^2 0.55, and LOOCV MAE 0.12, RMSE 0.15 and the squared correlation (R^2) of the predictions to the observations 0.57.

Table S3: Modern tree cover model coefficients, including %wind pollinated rather than %needleleaf

Coefficients (mean model with logit link)	**Estimate**	**Standard Error**	**P Value**
(Intercept)	-1.045	1.899	0.582
Tree pollen %	2.592	0.233	8.66e-29 ***
Shrub pollen %	-3.834	0.642	2.38e-09 ***
Wind pollination of AP%	-11.090	4.486	0.013 *
Wind pollination of AP%^2	7.264	2.701	0.007 **
AP Shannon index	4.413	0.481	4.61e-20 ***
AP Shannon index^2	-1.237	0.145	1.16e-17 ***
Lake or bog site	-0.034	0.139	0.807
Elevation	0.003	0.001	0.007 **
AP pollen:elevation interaction	-0.001	0.001	0.003 **
SP pollen:elevation interaction	0.004	0.001	0.003 **
AP Shannon:elevation interaction	-0.004	0.001	0.001 **
AP Shannon^2:elevation interaction	0.002	0.000	3.05e-05 ***
Lake or bog site:elevation interaction	-0.001	0.000	3.32e-04 ***
Precision submodel (log link; after variable selection^^)			
(Intercept)	-2.827	0.988	0.004 **
Wind pollination of AP%	3.382	0.978	5.41e-04 ***
AP Shannon index	0.938	0.116	4.84e-16 ***

Lake or bog site	0.537	0.126	1.97e-05 ***

Significance codes: 0 = '***'; 0.001 = '**'; 0.01 = '*'; 0.05 = '' 0.1; ' ' = 1

^^Only significant covariates were included (at 5% significance)

Similarly, including %*Pinus* within the model instead of %Needleleaf also slightly reduced the quality of the model fit, reducing the pseudo (Cox-Snell) R^2 to 0.59 (vs 0.60). Although the LOOCV MAE (0.11) and RMSE (0.14) were approximately the same as the model with %needleleaf, the squared correlation (R^2) of the predictions to the observations reduced slightly to 0.62 (from 0.63). The model coefficients are shown in Table S4. This slight reduction in model fit supports the use of %needleleaf, although this marginal difference suggests that %*Pinus* could also be used and tested for other geographic contexts.

Table S4: Modern tree cover model coefficients, including %Pinus pollinated rather than %needleleaf

Coefficients (mean model with logit link)	**Estimate**	**Standard Error**	**P Value**
(Intercept)	-6.008	0.453	3.91e-40 ***
Tree pollen %	2.428	0.222	1.47e-28 ***
Shrub pollen %	-3.539	0.629	1.82e-08 ***
Pinus of AP%	-0.010	0.005	0.04272 *
Pinus of AP%^2	0.000	0.000	2.77e-07 ***
AP Shannon index	5.530	0.482	1.77e-30 ***
AP Shannon index^2	-1.497	0.144	3.62e-25 ***
Lake or bog site	-0.039	0.133	0.76985
Elevation	0.002	0.001	0.045 *
AP pollen:elevation interaction	-0.001	0.000	0.029 *
SP pollen:elevation interaction	0.004	0.001	0.002 **
AP Shannon:elevation interaction	-0.003	0.001	0.002 **
AP Shannon^2:elevation interaction	0.001	0.000	3.65e-05 ***
Lake or bog site:elevation interaction	-0.001	0.000	0.002 **
Precision submodel (log link; after variable selection^^)			
(Intercept)	0.082	0.264	0.755
Pinus of AP%	0.013	0.003	8.62e-07 *
AP Shannon index	0.959	0.128	5.98e-14 ***
Lake or bog site	0.582	0.125	3.45e-06 ***

Section S4: Modern tree species diversity and tree cover

The tree pollen Shannon index (SI) is an important component of the regression model (Table 2). With increased tree cover, it is more likely that tree species diversity increases, although the negative second-degree polynomial (Table 1) suggests that at higher levels of tree cover this relationship becomes less important. To investigate this relationship, we divided the modelled modern data into biomes, and explore whether the SI for tree pollen varies for more open biomes. We divided the records into biomes according to Hengl's (2018) map of potential natural vegetation, extracting the modal biome with a 5km buffer around each record. We grouped some similar biomes, to simplify comparison; this grouping, and the division of modelled modern records, is shown in Table S5.

Table S5: Biome groups for included modelled modern records. Parenthesis indicates grouped biomes

Biome group (incl. biomes)	**Number of modern records**
Cool evergreen needleleaf forest (Cold evergreen needleleaf forest; cool evergreen needleleaf forest)	363
Cool mixed forest	255
Temperate deciduous broadleaf forest	117
Warm temperate evergreen and mixed forest	84
Tundra (Low and high shrub tundra; Erect dwarf shrub tundra)	29
Xerophytic scrub and woodlands (Steppe; Xerophytic woods scrub)	4

The distribution of arboreal pollen percentages and observed tree cover percentages are shown for each biome group in Fig. S1. In general, arboreal pollen percentages are greater than observed tree cover for each biome group, but the difference is most stark for the tundra biome (and xerophytic scrub and woodlands, although there are very few records). Figure S2 shows the arboreal pollen Shannon index values for each group. The lowest median value and distribution is for tundra, suggesting that the higher pollen values compared to observed cover reflects inputs from a few species through long-distance transport. In fact, it is generally the case that the larger the difference between arboreal pollen and observed tree cover percentages, the lower the tree SI value. This highlights the importance of including this variable in the regression model.

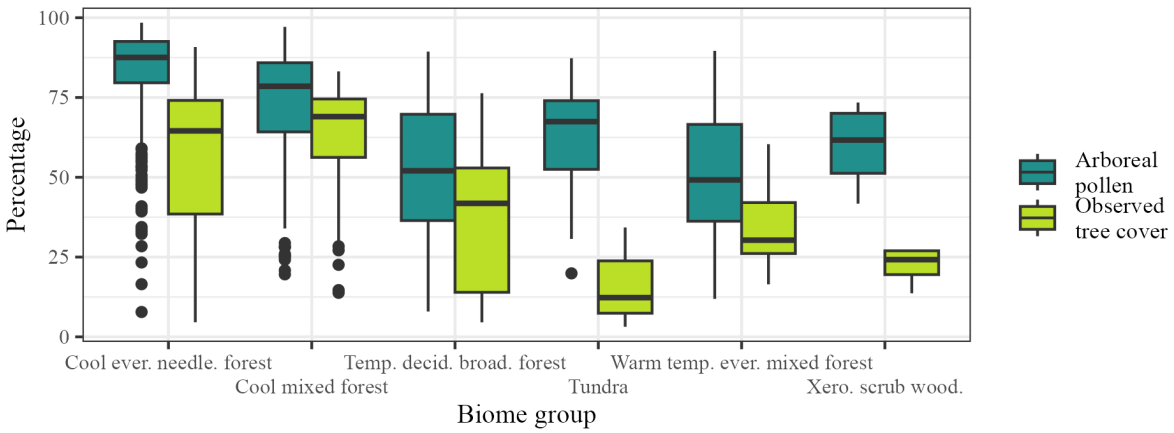

Figure S1: Boxplots of arboreal pollen and observed tree cover by biome group

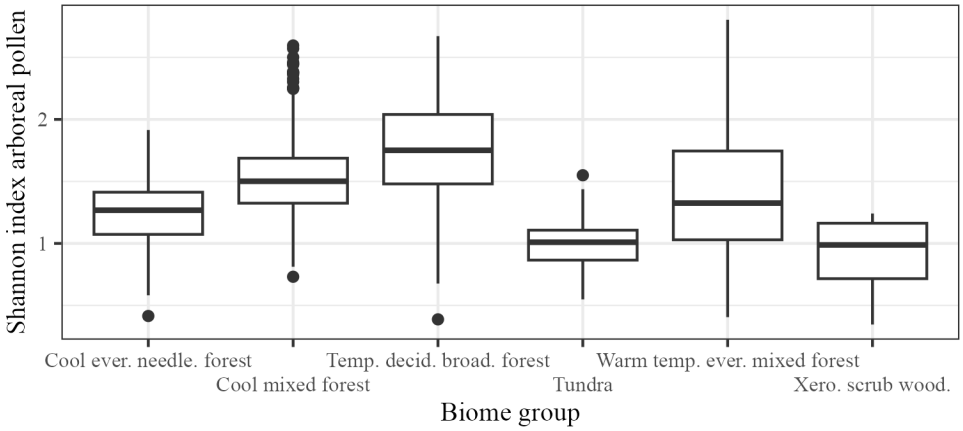

Figure S2: Boxplots of Shannon index values for tree pollen for each biome group

Section S5: Coefficients and model fit based on lake sites only

Excluding bog sites from model fit improves the LOOCV RMSE to 0.13 (vs. 0.14), MAE to 0.10 (vs. 0.11) and squared correlation (R^2) of the predictions and observations to 0.69 (vs. 0.63). The model coefficients are shown in Table S6. Coefficient estimates have the same direction as the model with bogs and lakes. Although the model fit improves, excluding bog sites from the model substantially reduces the applicability of the model to fossil records; lake records only constitute 35% of the total available fossil records.

Table S6: Modern tree cover model coefficients for lake sites only

Coefficients (mean model with logit link)	**Estimate**	**Standard Error**	**P Value**
(Intercept)	-5.421	0.444	3.05e-34 ***
Tree pollen %	2.169	0.247	1.55e-18 ***
Shrub pollen %	-4.613	0.759	1.25e-09 ***
Needle share of AP%	-1.546	0.529	0.004 **
Needle share of AP%^2	3.241	0.583	2.69e-08 ***
AP Shannon index	5.239	0.483	2.14e-27 ***
AP Shannon index^2	-1.421	0.146	1.65e-22 ***
Elevation	0.001	0.001	0.317
AP pollen:elevation interaction	-0.001	0.001	0.016 *
SP pollen:elevation interaction	0.005	0.002	0.003 **
AP Shannon:elevation interaction	-0.003	0.001	0.005 **
AP Shannon^2:elevation interaction	0.001	0.000	1.02e-04 ***
Precision submodel (log link; after variable selection^^)			
(Intercept)	1.089	0.257	2.26e-05 ***
Needle share of AP%	0.751	0.271	0.006 **
AP Shannon index	0.759	0.132	9.28e-09 ***

Significance codes: 0 = '***'; 0.001 = '**'; 0.01 = '*'; 0.05 = '' 0.1; ' ' = 1

^^Only significant covariates were included (at 5% significance)

Section S6: Coefficients and model fit without exclusion of sites >1000 m

Including higher elevation sites within the model reduces the LOOCV RMSE to 0.15 (vs. 0.14), MAE to 0.12 (vs. 0.11) and squared correlation (R^2) of the predictions and observations to 0.55 (vs. 0.63). The model coefficients are shown in Table S7. Coefficient estimates have the same direction as the model that excludes higher elevation sites, with the exception of the dummy variable for lake or bog site, which becomes negative and significant (from positive and insignificant), and the interaction between elevation and whether a site was a lake or bog, which becomes positive (but insignificant (from negative and significant). The significance of the coefficients improves in several cases, most notably for elevation which becomes highly significant having been insignificant when excluding higher elevation sites. Although including high elevation records increases the spatiotemporal coverage of the tree cover reconstruction – the number of fossil records increases from 811 to 1050 - the impact on model fit is such that we have much less confidence in the reconstructions.

Table S7: Modern tree cover model coefficients without exclusion of high (>1000 m) sites

Coefficients (mean model with logit link)	**Estimate**	**Standard Error**	**P Value**
(Intercept)	-5.249	0.346	6.26e-52 ***
Tree pollen %	2.447	0.178	6.58e-43 ***
Shrub pollen %	-3.044	0.495	7.92e-10 ***
Needle share of AP%	-1.599	0.418	1.28e-4 ***
Needle share of AP%^2	2.954	0.453	6.98e-11 ***
AP Shannon index	4.797	0.382	4.27e-36 ***
AP Shannon index^2	-1.214	0.117	2.39e-25 ***
Lake or bog site	-0.349	0.092	1.50e-4 ***
Elevation	0.002	3.74e-4	2.71e-6 ***
AP pollen:elevation interaction	-0.001	1.83e-4	1.76e-6 ***
SP pollen:elevation interaction	0.003	5.14e-4	4.62e-10 ***
AP Shannon:elevation interaction	-0.003	1.39e-4	3.59e-10 ***
AP Shannon^2:elevation interaction	0.003	5.14e-4	1.79e-11 ***
Lake or bog site:elevation interaction	0.000	8.08e-5	0.932
Precision submodel (log link; after variable selection^^)			
(Intercept)	1.146	0.228	4.81e-7 ***
Needle share of AP%	0.500	0.271	0.009 **
AP Shannon index	0.473	0.132	4.42e-6 ***
Lake or bog site	0.210	0.098	0.032 *

Significance codes: 0 = '***'; 0.001 = '**'; 0.01 = '*'; 0.05 = '' 0.1; ' ' = 1

^^Only significant covariates were included (at 5% significance)

Section S7: Coefficients and model fit with a <500m maximum elevation for sites

Limiting the maximum elevation to 500m rather than 1000m has no tangible effect on the LOOCV RMSE (0.14) or squared correlation (R^2) of the predictions and observations (0.63). The model coefficients are shown in Table S8. The direction of non-elevation coefficients are consistent with the model excluding sites at or above 1000m, with the exception of site type, which remains non-significant. The needleleaf share of AP is no longer significant in the model, but the positive quadratic term for needleleaf share remains. This implies that the negative influence of needleleaf at lower levels of needleleaf AP share is restricted to sites at the 500 to 1000m range. Limiting the included sites to those less than 500m means that elevation and all of the interaction terms with elevation are no longer significant. Reducing the upper elevation site limit to 500m reduces the number of fossil records available for reconstruction from 811 to 622.

Table S8: Modern tree cover model coefficients excluding sites >500m

Coefficients (mean model with logit link)	**Estimate**	**Standard Error**	**P Value**
(Intercept)	-4.638	0.618	6.28e-14 ***
Tree pollen %	2.231	0.301	1.23e-13 ***
Shrub pollen %	-3.653	0.812	6.74e-6 ***
Needle share of AP%	-0.796	0.592	0.178
Needle share of AP%^2	2.419	0.652	2.06e-4 ***
AP Shannon index	4.041	0.672	1.76e-9 ***
AP Shannon index^2	-1.100	0.207	1.10e-7 ***
Lake or bog site	-0.011	0.183	0.952
Elevation	-0.003	0.002	0.173
AP pollen:elevation interaction	0.000	0.001	0.797
SP pollen:elevation interaction	0.006	0.003	0.073’
AP Shannon:elevation interaction	0.002	0.003	0.480
AP Shannon^2:elevation interaction	0.000	0.001	0.978
Lake or bog site:elevation interaction	-0.001	0.001	0.340
Precision submodel (log link; after variable selection^^)			
(Intercept)	0.133	0.309	0.667
Needle share of AP%	1.130	0.276	4.12e-05 ***
AP Shannon index	0.820	0.145	1.43e-08 ***
Lake or bog site	0.729	0.163	7.35e-06 ***

Significance codes: 0 = '***'; 0.001 = '**'; 0.01 = '*'; 0.05 = '’' 0.1; ' ' = 1

^^Only significant covariates were included (at 5% significance)

Section S8: Excluding crop cells from the calculation of observed tree cover

Cells dominated by crop cover (>50%) were excluded from the forest/tree cover map that was used to calculate observed tree cover for each modern pollen record. The rationale behind this methodological choice was to try to ensure that the relationship between tree cover and modern pollen was as representative as possible. Areas with high crop cover may affect the subsequent regression model, implying lower observed tree cover which is not reflected in the pollen record. To explore the implications of this exclusion, we re-ran the same regression model without excluding cells dominated by crop cover. The direction of the model coefficients (Table S9) are the same as the standard regression model, except for whether the site was a bog or lake (which now becomes significant). However, some variables, such as the shrub pollen %, and the interactions between AP pollen and elevation, and SP pollen and elevation, are no longer significant. Note that although the needleleaf share of AP% is also insignificant, a model with orthogonal polynomials (i.e. reducing multicollinearity with the second polynomial of needle share of AP%) is significant. Additionally, the needleleaf share of AP% and whether the site is a lake or bog are no longer significant in the precision sub-model.

Table S9: Modern tree cover model coefficients, without exclusion of crop dominated cells when calculating observed tree cover

Coefficients (mean model with logit link)	**Estimate**	**Standard Error**	**P Value**
(Intercept)	-5.068	0.405	5.38e-36 ***
Tree pollen %	2.199	0.186	3.01e-32 ***
Shrub pollen %	-0.731	0.508	0.150
Needle share of AP%	-0.031	0.433	0.943
Needle share of AP%^2	1.480	0.499	0.003 **
AP Shannon index	3.576	0.483	1.36e-13 ***
AP Shannon index^2	-1.085	0.153	1.25e-12 ***
Lake or bog site	0.386	0.095	5.04e-05 ***
Elevation	0.002	0.001	0.046 *
AP pollen:elevation interaction	-0.001	0.000	0.110
SP pollen:elevation interaction	0.000	0.001	0.624
AP Shannon:elevation interaction	-0.003	0.001	0.012 *
AP Shannon^2:elevation interaction	0.001	0.000	6.74e-05 ***
Lake or bog site:elevation interaction	-0.001	0.000	6.70e-09 ***
Precision submodel (log link; after variable selection^^)			
(Intercept)	1.459	0.230	2.4e-10 ***
Needle share of AP%	1.191	0.205	0.351

AP Shannon index	0.406	0.108	1.74e-04 ***
Lake or bog site	-0.039	0.107	0.714

Significance codes: 0 = '***'; 0.001 = '**'; 0.01 = '*'; 0.05 = '' 0.1; ' ' = 1

^^Only significant covariates were included (at 5% significance)

The model that does not exclude cells with >50% crops includes more records (1050 compared to 852) but the pseudo (Cox-Snell) R^2 model fit was worse than the standard model (0.47 compared to 0.60), with LOOCV values similarly worse (MAE = 0.13 vs 0.11; RMSE = 0.16 vs 0.14; R^2 of predictions to observations = 0.50 vs 0.63).

Section S9: Adjusting the source area based on different source pollen percentages

The source area used to calculate the observed tree cover values for each record is based on the source area for 70% of pollen, applied to Prentice's (1985) source area formula. To test the implications of different source areas using different proportions of pollen, we re-ran the modern tree cover regression with recalculated average tree cover using 50% and 35% of pollen. As the selection of records to include within the regression was restricted to those records with less than half of the contributing grid cells masked as land-cover classes other than vegetation, changing the size of the source areas affected the number of records included within the regression. With 50% of pollen, the number of records increased to 933 (from 852); with 35% of pollen this number 934. The regression coefficients for the two different percentages of pollen are shown in Tables S10 and S11.

Table S10: Modern tree cover model coefficients, with 50% of pollen used to calculate source area rather than 70%

Coefficients (mean model with logit link)	**Estimate**	**Standard Error**	**P Value**
(Intercept)	-5.298	0.413	1.08e-37 ***
Tree pollen %	2.577	0.222	2.85e-31 ***
Shrub pollen %	-2.855	0.597	1.75e-06 ***
Needle share of AP%	-1.700	0.477	3.69e-04 ***
Needle share of AP%^2	3.504	0.548	1.57e-10 ***
AP Shannon index	4.569	0.476	8.63e-22 ***
AP Shannon index^2	-1.238	0.151	1.96e-16 ***
Lake or bog site	0.147	0.125	0.241
Elevation	0.001	0.001	0.179
AP pollen:elevation interaction	-0.001	0.000	0.053 `
SP pollen:elevation interaction	0.002	0.001	0.048 *
AP Shannon:elevation interaction	-0.002	0.001	0.040 *
AP Shannon^2:elevation interaction	0.001	0.000	0.002 **
Lake or bog site:elevation interaction	-0.001	0.000	2.25e-05 ***
Precision submodel (log link; after variable selection^^)			
(Intercept)	0.680	0.240	0.005 **
Needle share of AP%	0.328	0.217	0.130
AP Shannon index	0.519	0.113	4.29e-06 ***
Lake or bog site	0.681	0.114	2.50e-09 ***

Significance codes: 0 = '***'; 0.001 = '**'; 0.01 = '*'; 0.05 = '' 0.1; ' ' = 1

^^Only significant covariates were included (at 5% significance)

The regression coefficient for both the 50% and 35% thresholds (Tables S10 and S11) the same sign as the 70% of pollen regression model but the significance of some of the predictors changes. Elevation and, the interaction between AP and elevation are no longer significant in both alternative models. Additionally, the needleleaf share of AP% is no longer significant within the precision sub-model. Overall, the 50% pollen model has a slightly worse fit, with a pseudo (Cox-Snell) R^2 of 0.58 (vs. 0.60), and LOOCV MAE of 0.12 (vs. 0.11), RMSE of 0.16 (vs.0.14) and squared correlation (R^2) between observed and predicted values of 0.61 (vs. 0.63). Similarly, the 35% pollen model has a worse fit, with a pseudo R^2 of 0.52, and LOOCV MAE of 0.14, RMSE of 0.17 and squared correlation (R^2) between observed and predicted values of 0.55.

Table S11: Modern tree cover model coefficients, with 35% of pollen used to calculate source area rather than 70%

Coefficients (mean model with logit link)	**Estimate**	**Standard Error**	**P Value**
(Intercept)	-5.537	0.473	1.20e-31 ***
Tree pollen %	2.524	0.254	2.72e-23 ***
Shrub pollen %	-3.132	0.645	1.21e-06 ***
Needle share of AP%	-1.954	0.551	3.90e-04 ***
Needle share of AP%^2	3.814	0.639	2.46e-09 ***
AP Shannon index	5.169	0.553	8.78e-21 ***
AP Shannon index^2	-1.459	0.175	8.20e-17 ***
Lake or bog site	0.122	0.141	0.388
Elevation	0.002	0.001	0.059 `
AP pollen:elevation interaction	-0.001	0.001	0.219
SP pollen:elevation interaction	0.003	0.001	0.028 *
AP Shannon:elevation interaction	-0.004	0.001	0.003 **
AP Shannon^2:elevation interaction	0.002	0.000	5.41e-05 ***
Lake or bog site:elevation interaction	-0.001	0.000	0.001 **
Precision submodel (log link; after variable selection^^)			
(Intercept)	0.441	0.233	0.058 `
Needle share of AP%	0.033	0.211	0.876
AP Shannon index	0.482	0.110	1.29e-05 ***
Lake or bog site	0.733	0.110	2.89e-11 ***

Significance codes: 0 = '***'; 0.001 = '**'; 0.01 = '*'; 0.05 = '' 0.1; ' ' = 1

^^Only significant covariates were included (at 5% significance)

Section S10: Quantile mapping influence on model predictions

Figure S3 (A–D) shows the impact of applying a quantile mapping model to the modern tree cover predictions solely based on the model of modern tree cover. The quantile mapping approach is designed to identify a transformation that matches the distribution of adjusted predictions to that of the observations (Gudmundsson et al., 2012). We used a smoothing spline regression curve to model the transformation, with the resulting calibration curve used to adjust modern and fossil pollen tree cover reconstructions, based on the approach from the R package *qmap* (Gudmundsson et al., 2012; version 1.0-6) and following Zanon et al. (2018). At the lower and higher levels of observed cover, quantile mapping reduces the respective over- and under-estimation.

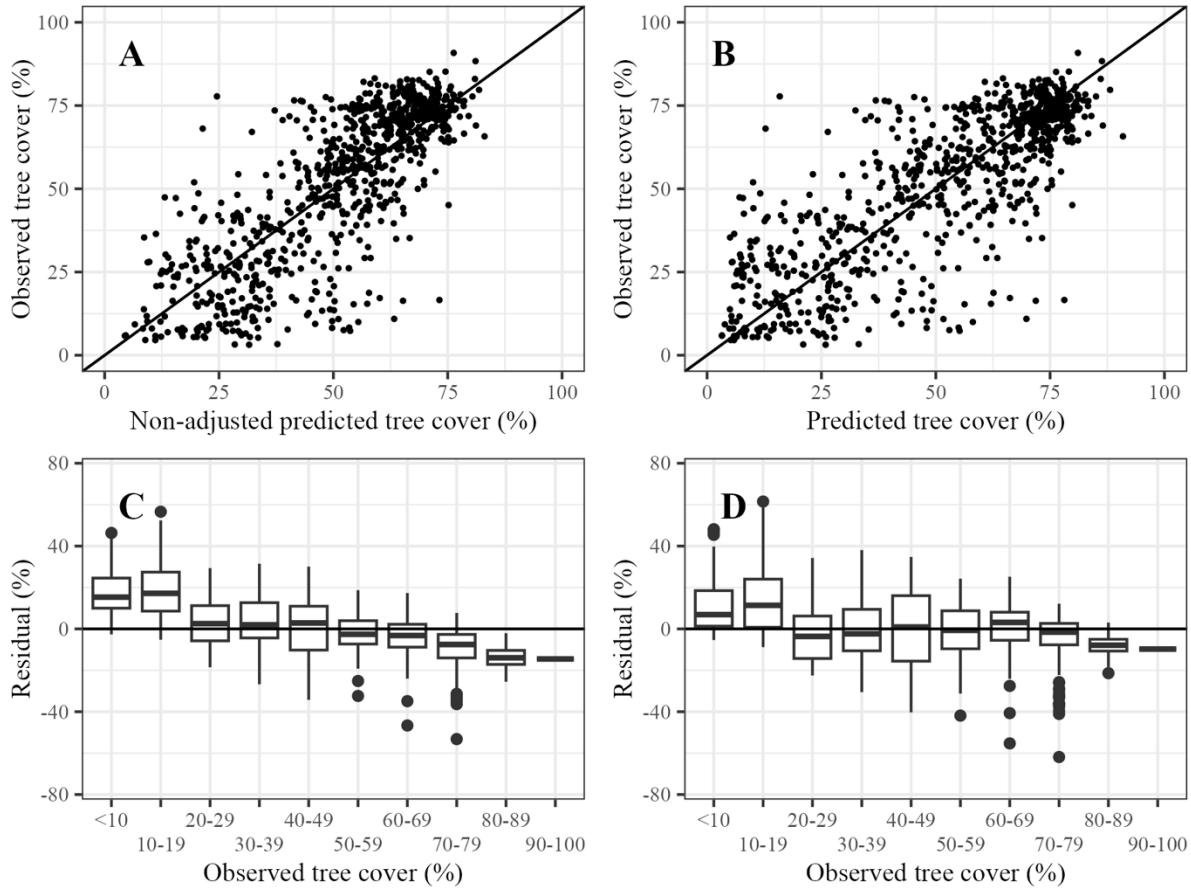

Figure S3: Model performance: A – Non-adjusted predictions of tree cover compared to observed tree cover; B - Predictions of tree cover compared with observed tree cover; C - Differences between non-adjusted predictions and observations (residual), in bins of observed tree cover percentage; D - Differences between predictions and observations (residual), in bins of observed tree cover percentage.

Section S11: Spatial structure of model predictions compared to observations

Figure S4 is a 50km^2 map showing the grid cell averaged differences between the model predictions adjusted by quantile mapping, and observations. Difference refers to predictions minus observations. In general, there is no spatial patterning in the location of overestimates, except that there is a tendency for a grouping of cells with overestimates in the far north of Scandinavia and some sites in Ireland.

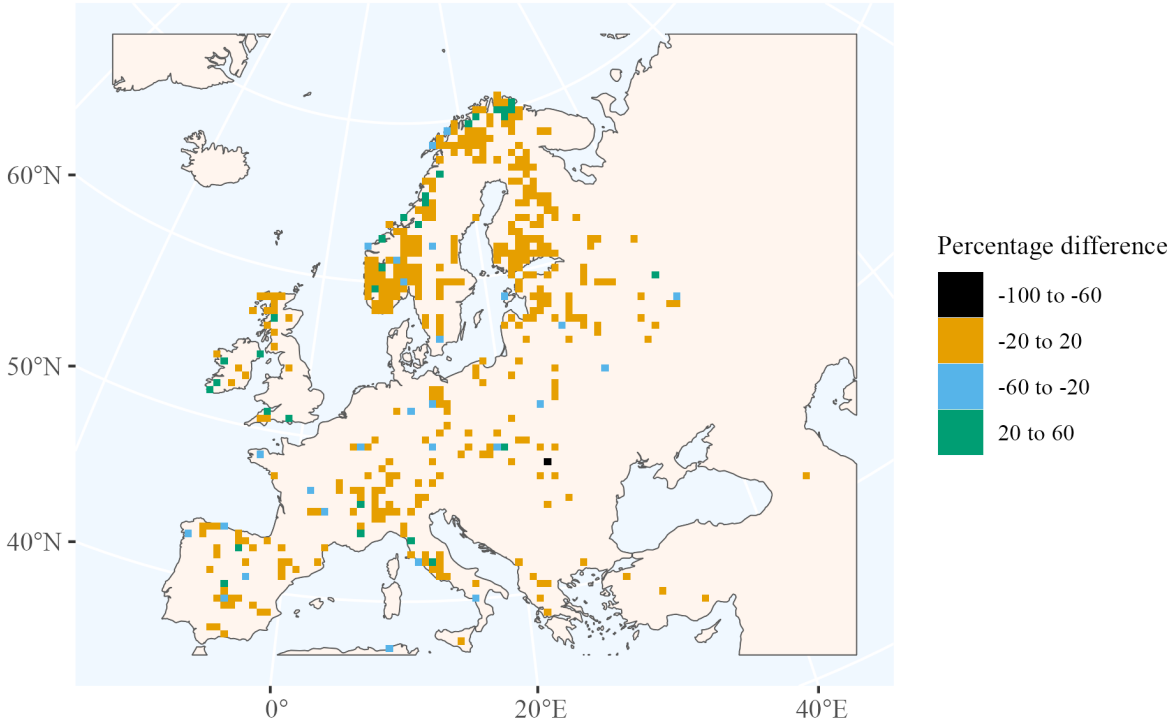

Figure S4: Spatial structure of differences between predictions and observations.

Section S12: Arboreal pollen percentages compared with observed tree cover percentages

Raw arboreal pollen percentages tend to overestimate tree cover, with the range in AP% greater for lower observed tree cover groups (Fig. S5).

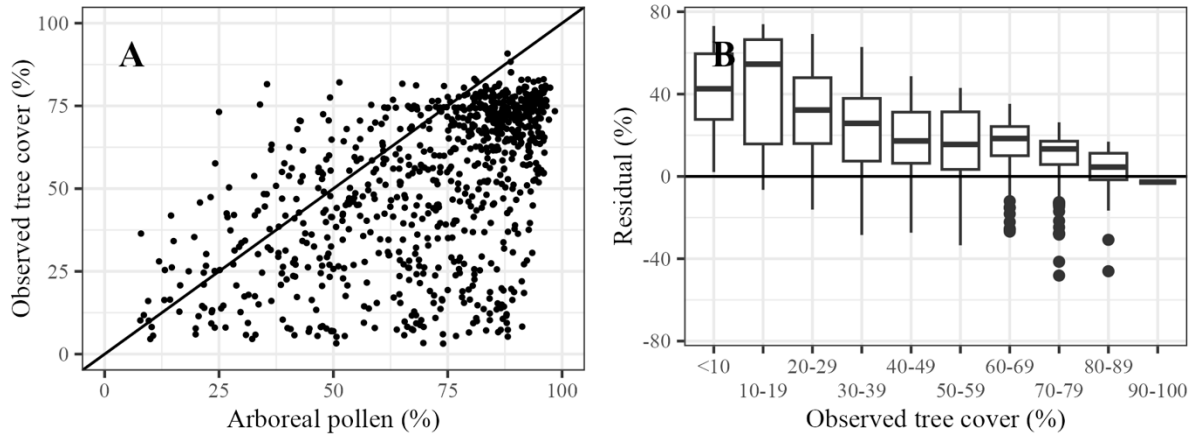

Figure S5: Arboreal pollen percentage compared to observed tree cover: A - AP% compared to observed tree cover for each record; B - Differences between AP% and observations (residual), in bins of observed tree cover percentage

Section S13: Modern predictions compared with other reconstructions based on grid cell averages

Figure S6 (A–D) shows the relationship between observations of tree cover and our predictions of tree cover compared with values extracted from the first bin of Zanon et al. (2018) and Serge et al. (2023) at the same spatial locations. Compared with Fig. 4, Fig. S6 averages tree cover values for each record by grid cell of the other reconstructions. Hence a single point in each panel may represent tree cover value for multiple records, if there were multiple records sharing a grid cell. There are less points within panels C and D compared to A and B because Serge et al. (2023) data is provided at much lower spatial resolution than Zanon et al. (2018) data.

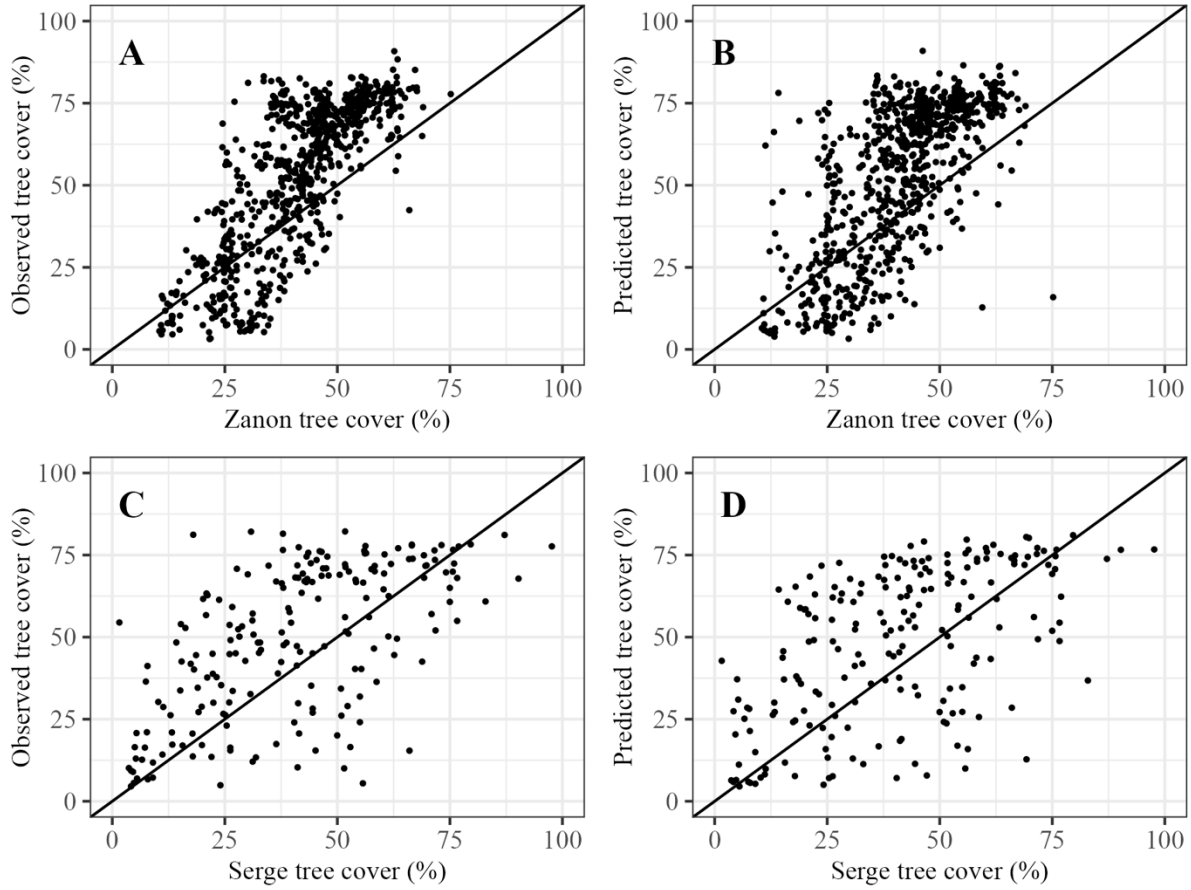

Figure S6: Modern tree cover from Zanon et al (2018) per grid cell compared to (A) observed tree cover and (B) our predicted tree cover. Modern tree cover from Serge et al. (2023) per grid cell compared to (C) observed tree cover values and (D) our predicted tree cover.

Section S14: Mean reconstructed tree cover

The influence of using mean tree cover values rather than median values to describe tree cover changes through time is shown in Fig. S7. Compared to the median (Fig. 5), the maximum and minimum tree cover values are reduced, and the variation through time is more limited. However, the structure of the trend through time in tree cover remains the same.

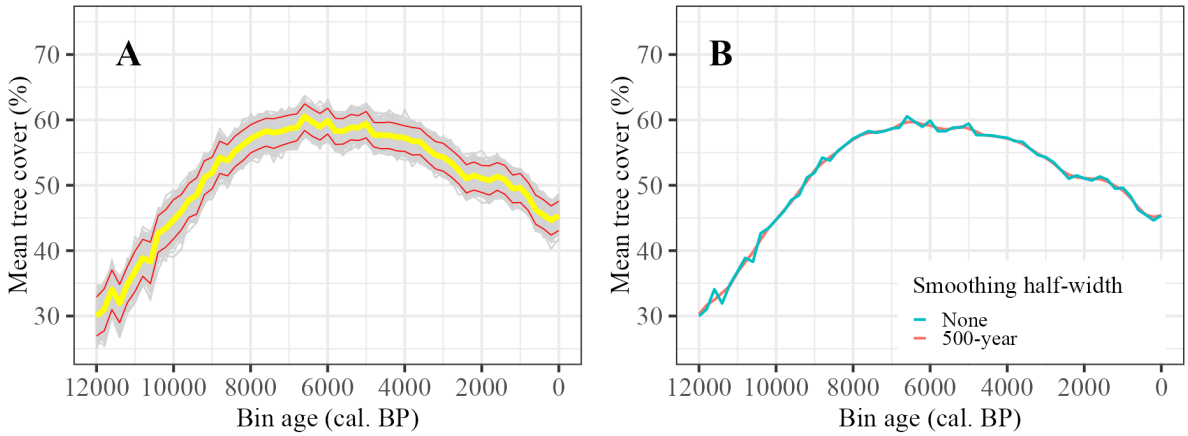

Figure S7: A - Mean reconstructed tree cover for Europe from 12,000 to 0 cal. BP, with 95% confidence intervals for 1000 bootstrap resampling of records; B - Mean reconstructed tree cover for Europe from 12,000 to 0 cal. BP, with differing LOESS regression smoothing half-widths.

Section S15: Median reconstructed tree cover, with bootstrapped models

To generate reconstruction standard errors, the predictive model that linked observed tree cover to modern pollen data was generated 1000 times by bootstrapping the modern pollen data. These models were also used to generate the equivalent number of quantile mapping adjustments, by relating model predictions using the full dataset to observations. Together these elements were used to produce 1000 different reconstructions of tree cover for each fossil data sample, with prediction standard error calculated by sample and averaged by 200-year bin. As well as using the bootstrapped reconstructions to generate the standard error, we can use the median of these bootstraps as another way of assessing the confidence in the median reconstruction. Figure S8 shows the median tree cover estimate, together with the bootstrapped medians of tree cover based on the different models and quantile mapping adjustment generated. Although the bootstrapped medians follow the same general pattern as the reconstructed median, maximum tree cover values for the reconstruction are generally higher than the bootstrapped medians, implying that some training samples may have a larger influence on the generated model than others.

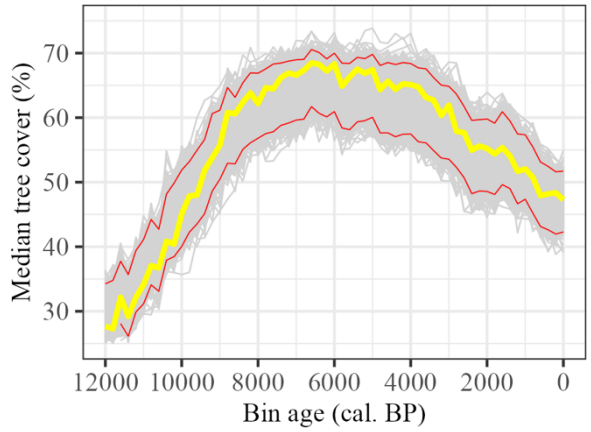

Figure S8: Median reconstructed tree cover for Europe from 12,000 to 0 cal. BP, with 95% confidence intervals for models generated through 1000 bootstrap resamples of model training data

Section S16: AP Shannon index through time and implications for tree cover reconstructions

The Shannon index (SI) value of arboreal pollen has a substantial impact on the quality of the model fit (Table 2). To investigate the implications of this variable for tree cover reconstructions, we re-ran the downcore reconstructions based on a model excluding tree cover SI (Fig. S9B) compared to the original model (Fig. S9A). Although the general mid-Holocene peak is visible in both reconstructions, there are differences between the two models. At the beginning of the Holocene, the median tree cover is around 20% higher when excluding tree SI. As a result, the increase in tree cover to the mid-Holocene is less dramatic. Additionally, the peak in tree cover occurs earlier, between ca. 9,000 and 7,000 cal. BP, compared to ca. 6,000 cal. BP when including the tree SI. In addition, the median tree cover values towards the present are around 5% lower when excluding tree SI.

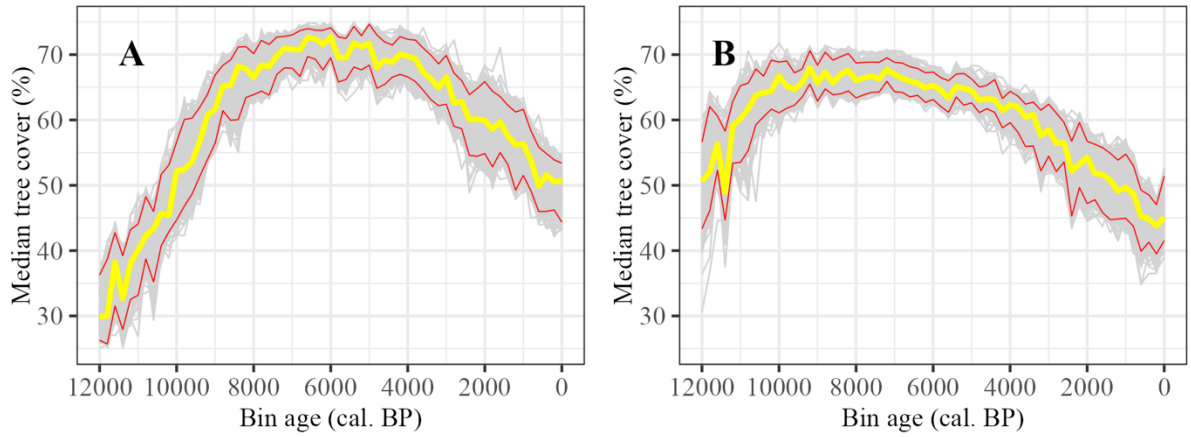

Figure S9: A - Median reconstructed tree cover for Europe from 12,000 to 0 cal. BP, with 95% confidence intervals for 1000 bootstrap resampling of records; B - Median reconstructed tree cover for Europe from 12,000 to 0 cal. BP excluding AP Shannon index, with 95% confidence intervals for 1000 bootstrap resampling of records

The tree SI values generally increased from the early Holocene to ca. 7,000 cal. BP (Fig. S10) and then remain relatively stable. Given that the tree SI has a positive relationship with observed tree cover in the modern regression model, this may imply that tree cover predictions for this earlier period of the Holocene are underestimated. However, since tree SI values are a means to correct for long distance transport, it is more likely that this implies there were more open environments earlier in the Holocene than is now the case.

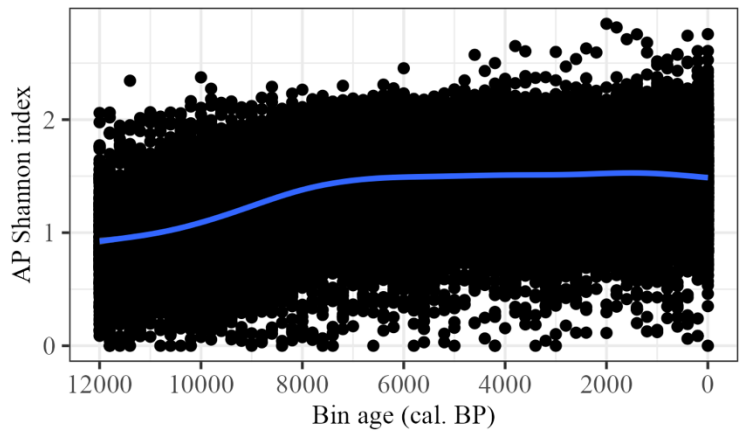

Figure S10: AP Shannon index for Europe from 12,000 to 0 cal. BP, average for individual records binned in 200-year bins. Blue line is a LOESS line of best fit

Section S17: Gridded maps of reconstructed tree cover through time

Gridded maps of reconstructed tree cover are shown below. The values in each cell are the mean of binned tree cover reconstructions for records located in each 50km^2 grid cell. Bins are 200-years in width, with ages referring to mid-point of each bin (e.g. the bin labelled 12,600 cal. BP represents the interval 12,700–12,500 cal. BP).

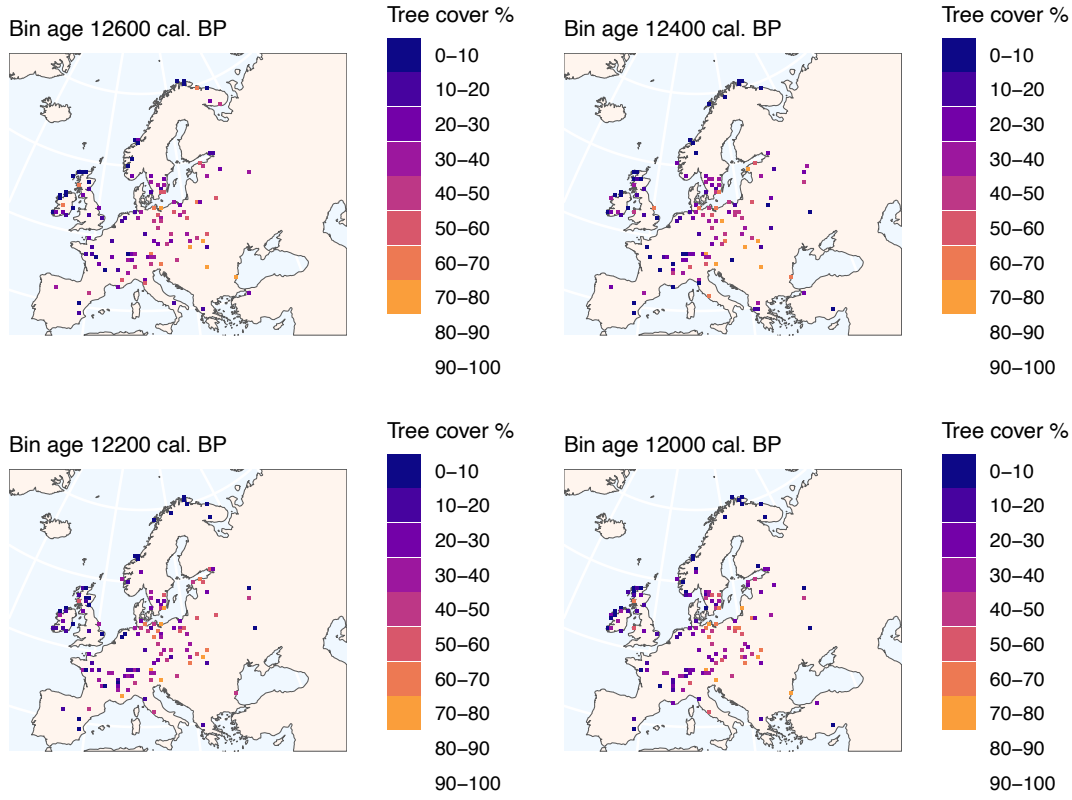

Figure S11: Gridded maps of reconstructed tree cover: 12,600 – 12,000 cal. BP

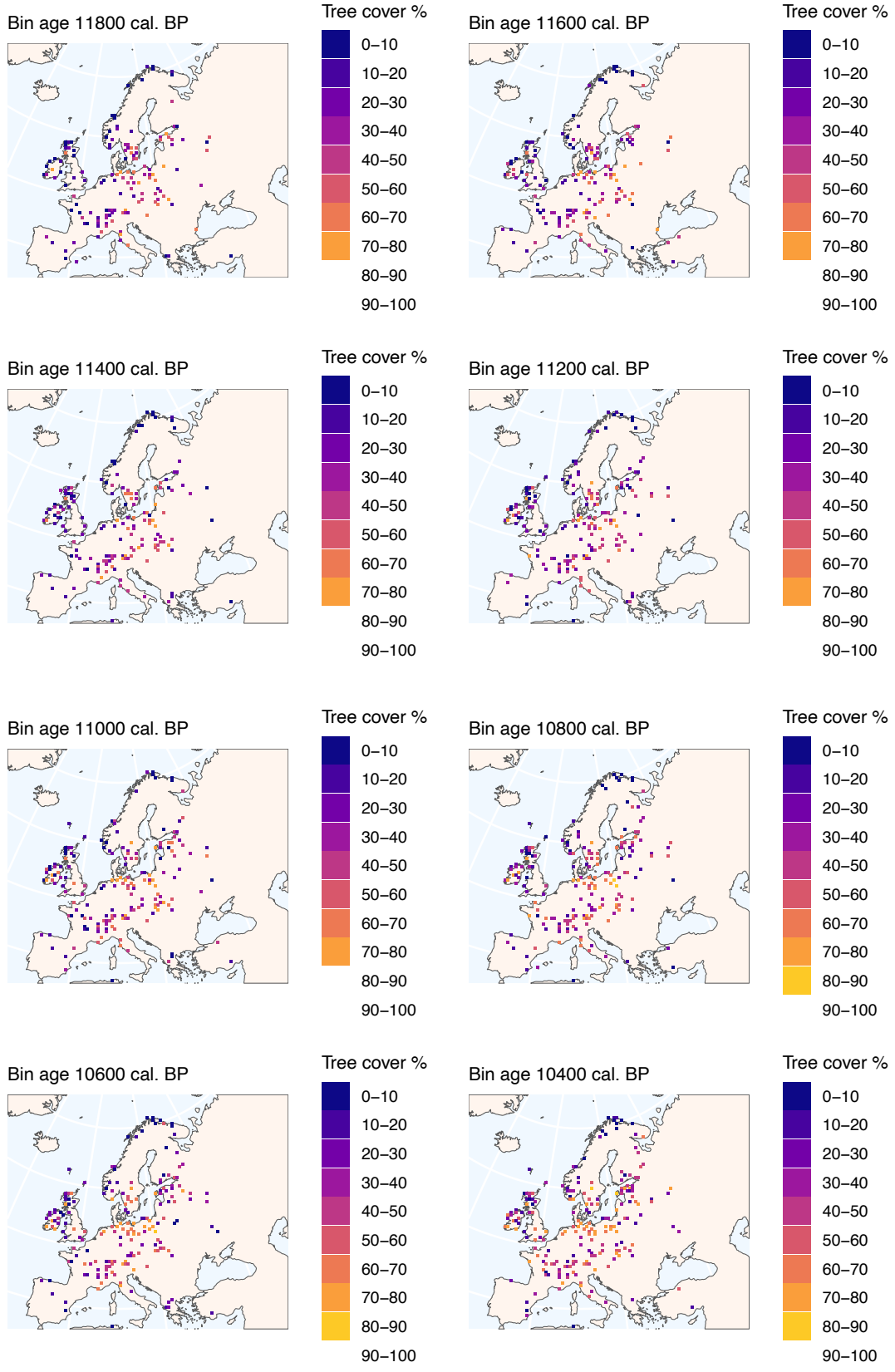

Figure S12: Gridded maps of reconstructed tree cover: 11,800 – 10,400 cal. BP

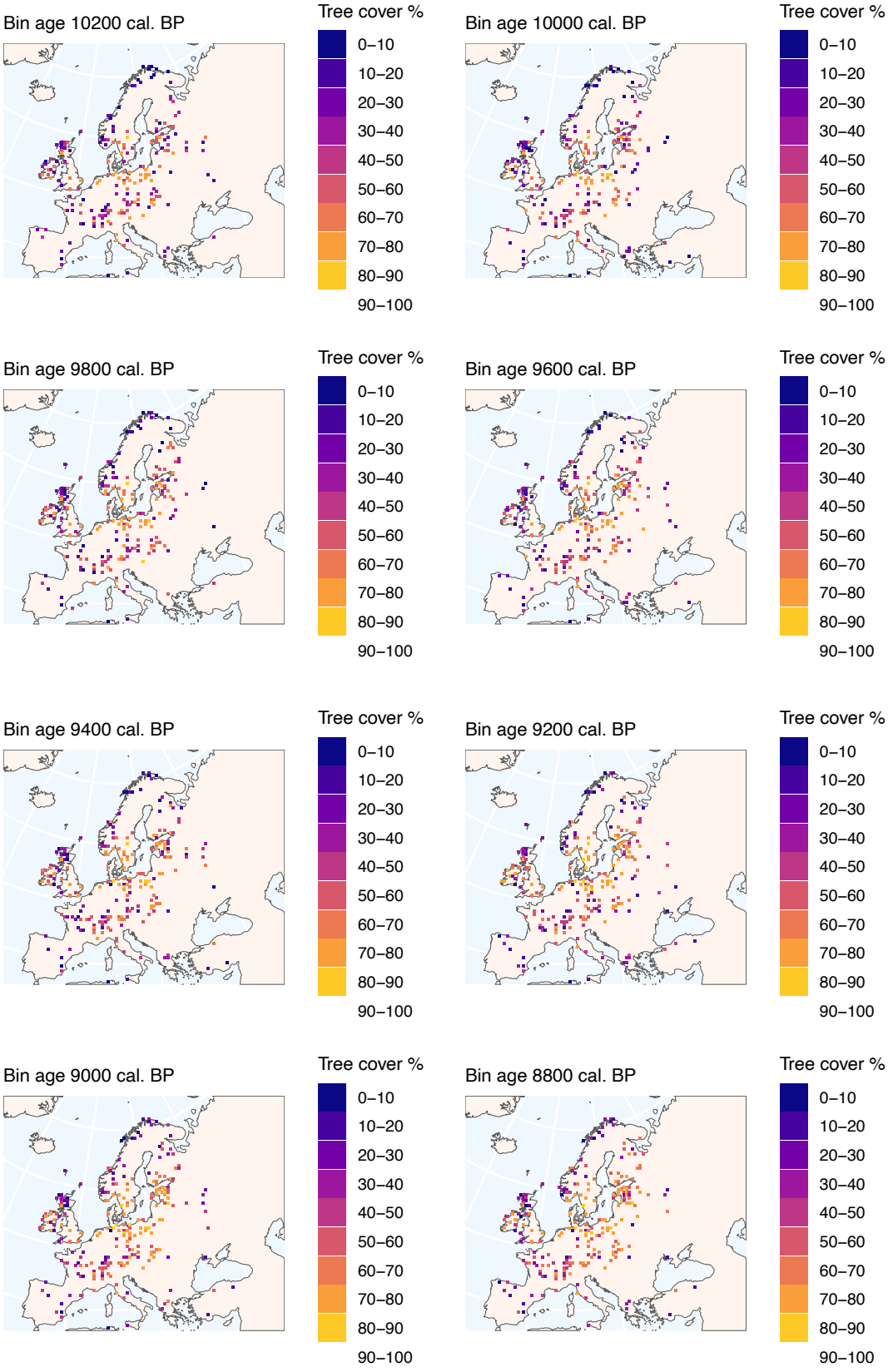

Figure S13: Gridded maps of reconstructed tree cover: 10,200 – 8,800 cal. BP

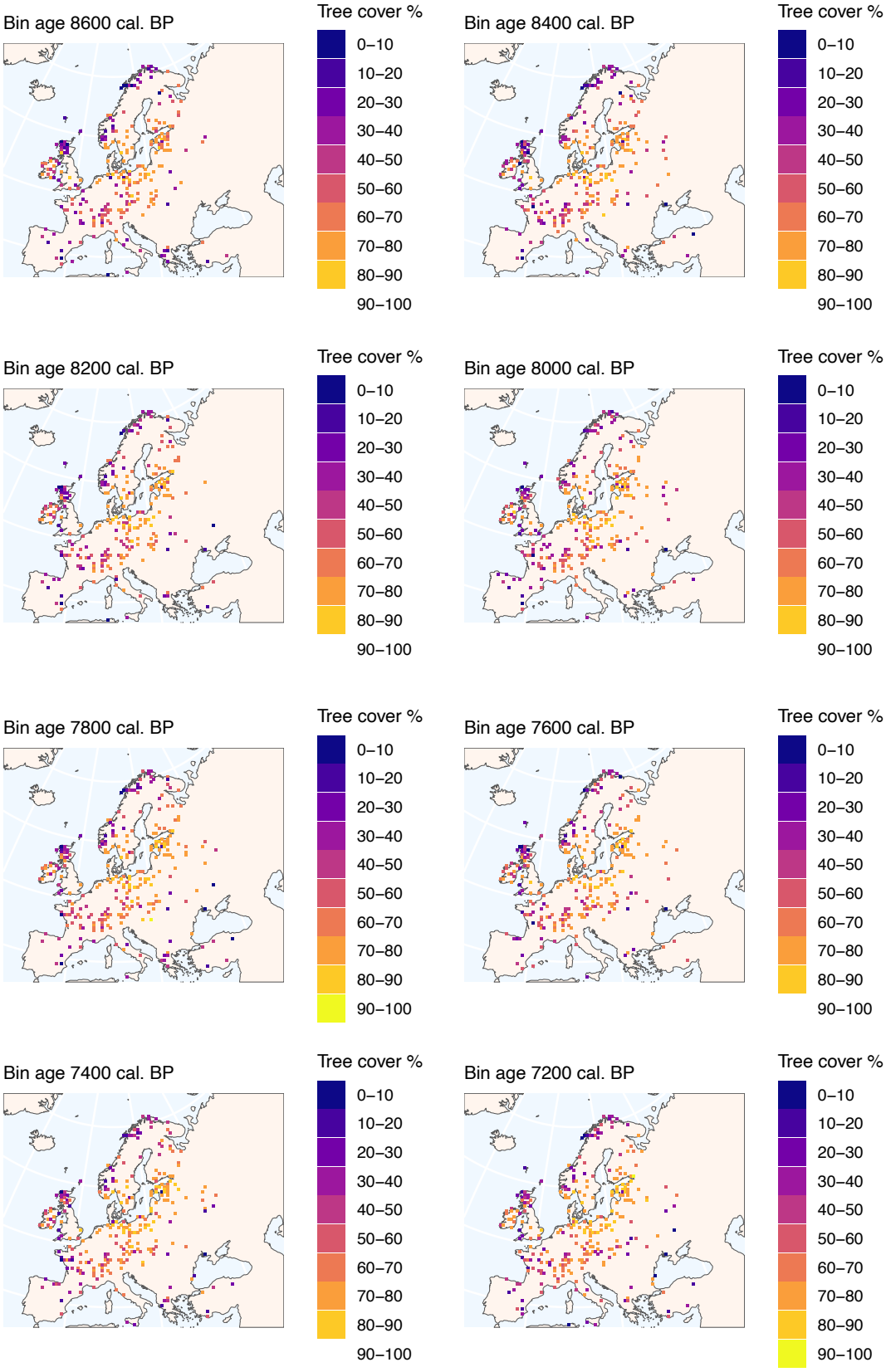

Figure S14: Gridded maps of reconstructed tree cover: 8,600– 7,200 cal. BP

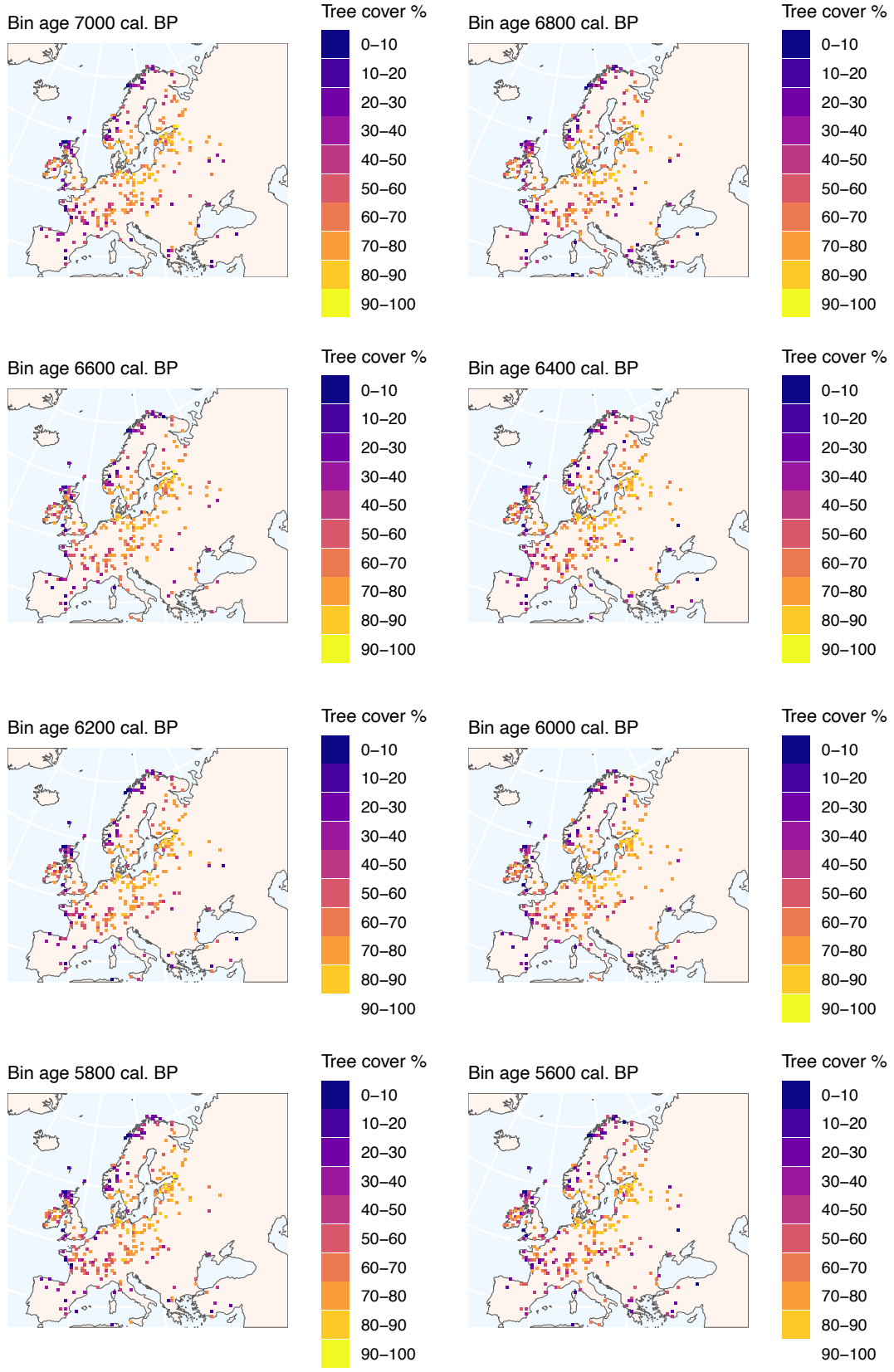

Figure S15: Gridded maps of reconstructed tree cover: 7,000 – 5,600 cal. BP

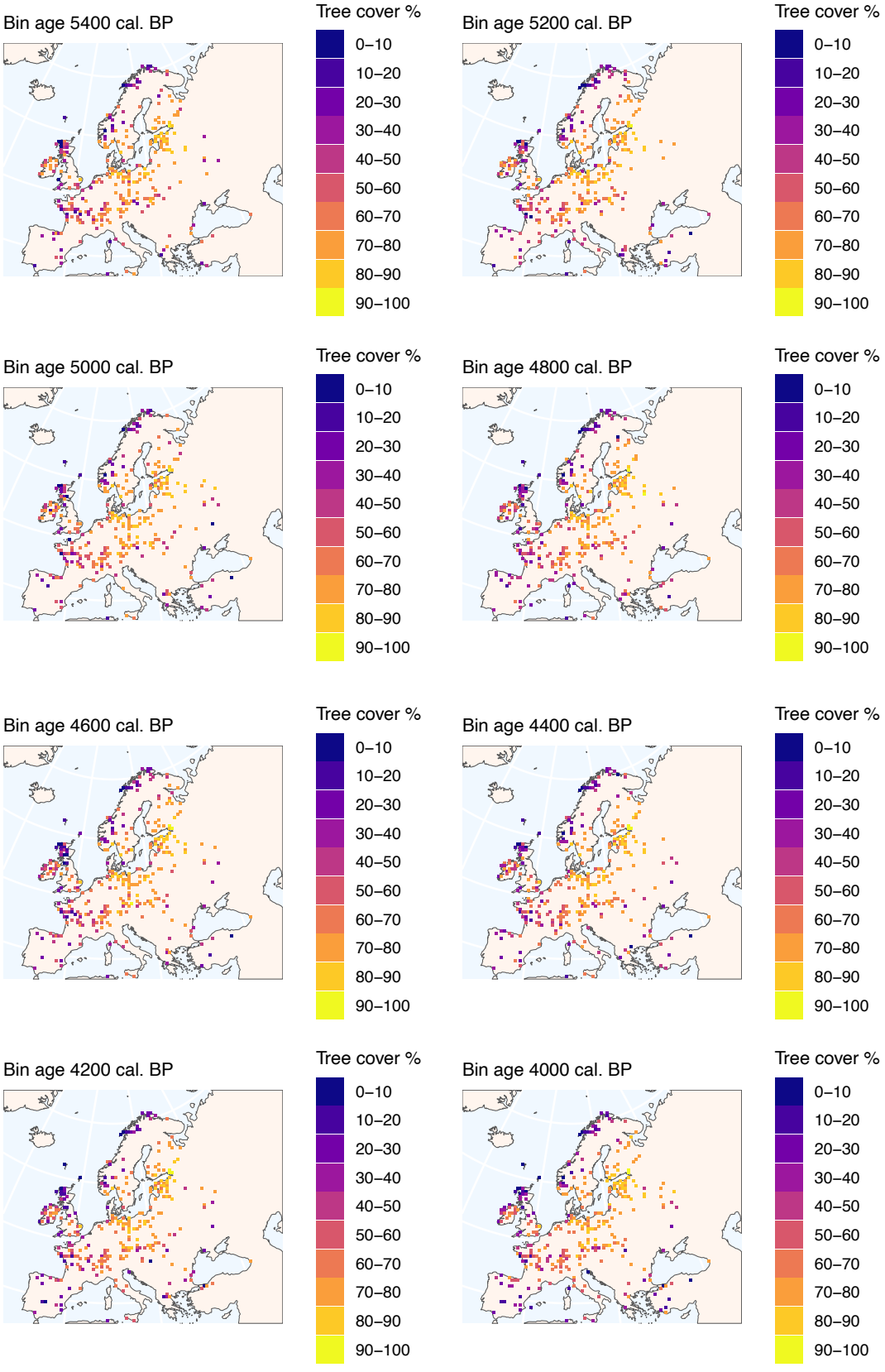

Figure S16: Gridded maps of reconstructed tree cover: 5,400 – 4,000 cal. BP

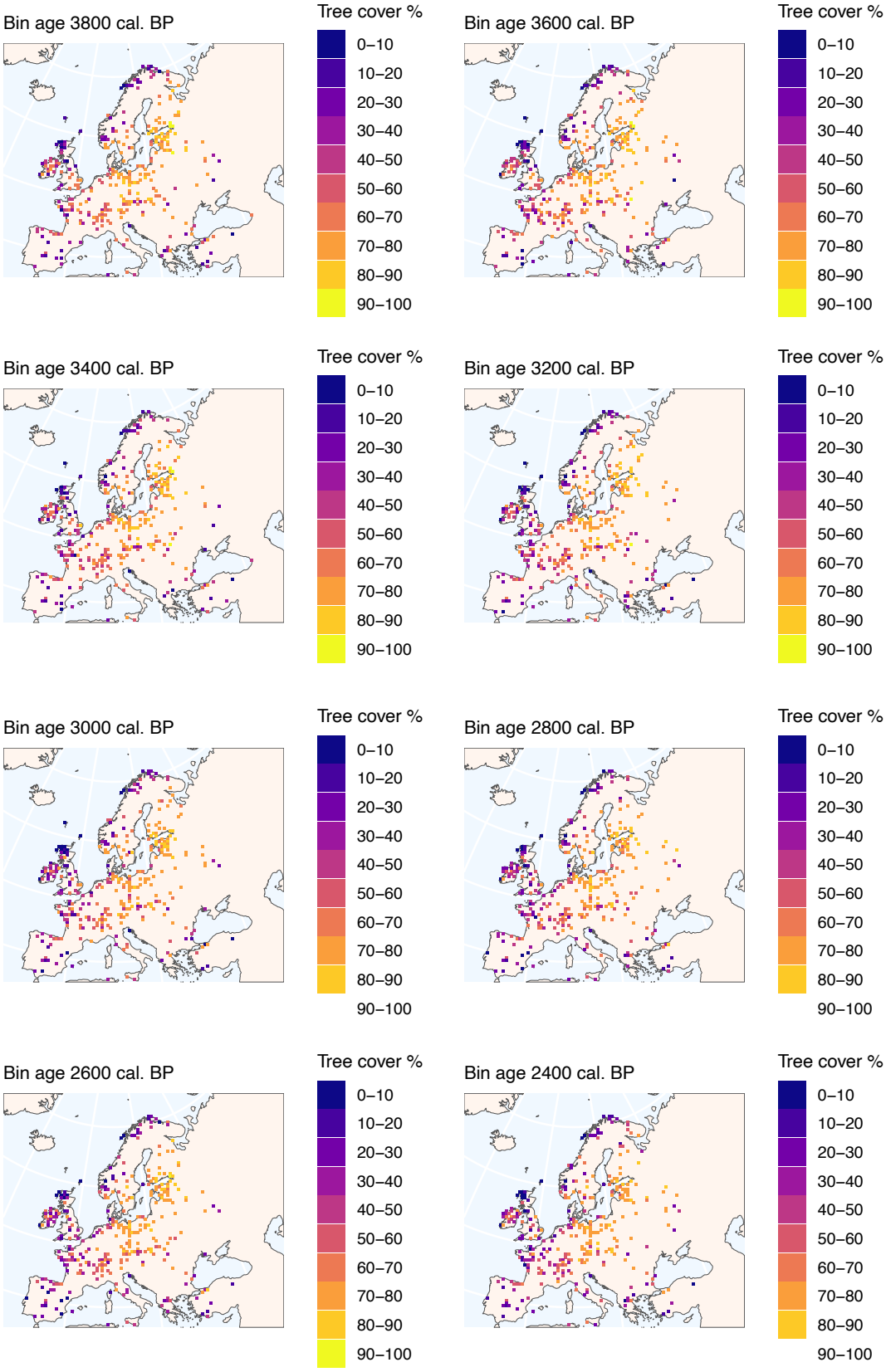

Figure S17: Gridded maps of reconstructed tree cover: 3,800 – 2,400 cal. BP

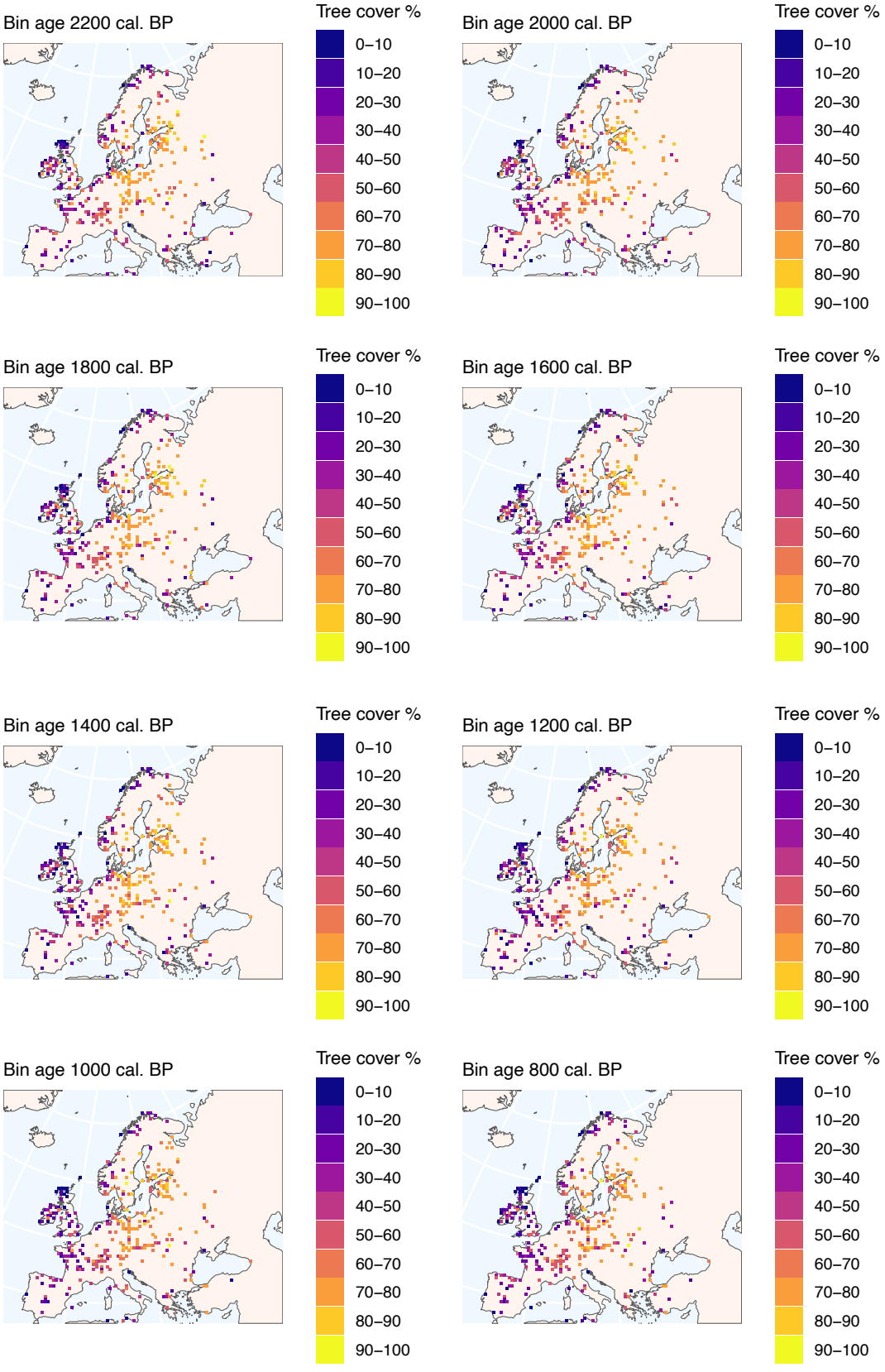

Figure S18: Gridded maps of reconstructed tree cover: 2,200 – 800 cal. BP

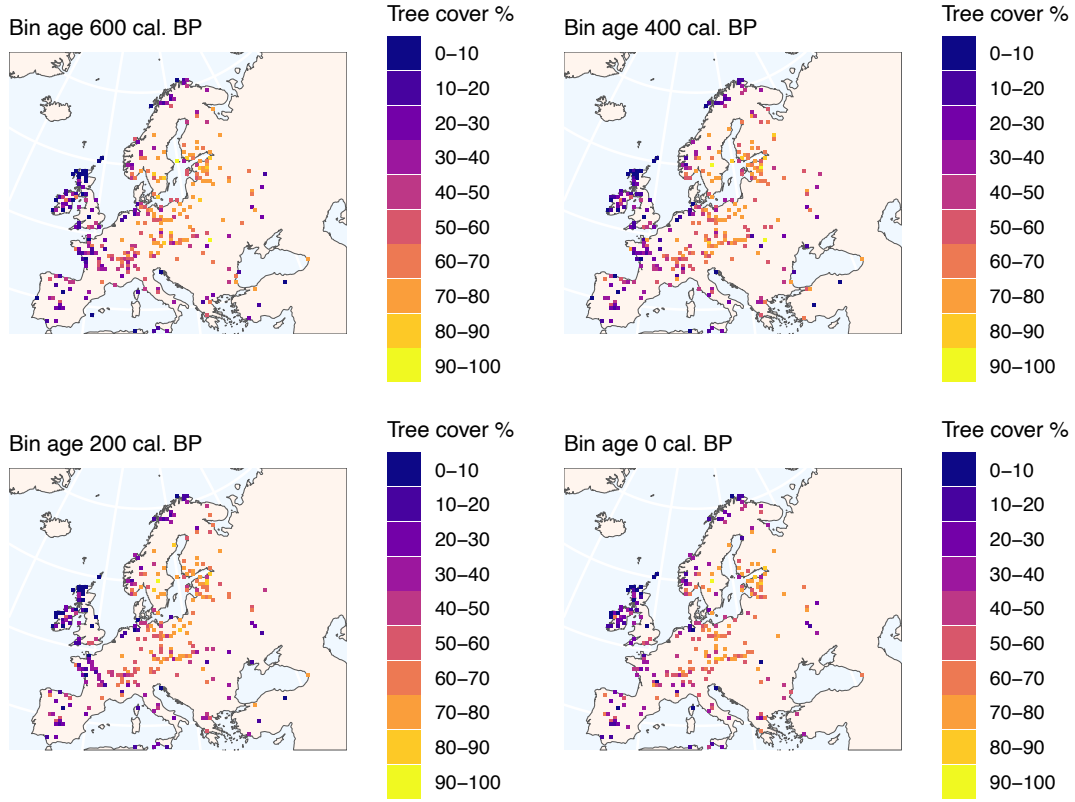

Figure S19: Gridded maps of reconstructed tree cover: 600 – 0 cal. BP

Section S18: Data by biogeographical region

Table S12 shows the breakdown of fossil pollen data by biogeographical region, with the number of records and the number of samples by 200-year bin within each region. Biogeographical regions are based on the European Environment Agency modern classification (European Environment Agency, 2016).

Table S12: Data by biogeographical region

Bioregion	**Number of records**	**Number of temporal bins**
Alpine	67	2377
Anatolian	3	75
Arctic	7	279
Atlantic	284	7117
BlackSea	6	157
Boreal	137	4127
Continental	219	6840
Mediterranean	73	1701
Pannonian	13	368
Steppic	1	38

Section S19: Median reconstructed tree cover based on bin widths from other reconstructions

The different tree cover reconstructions use different temporal bins, which can have an influence on our reconstructed median tree cover. Figure S20 shows our median tree cover reconstruction based on a standard 200-year bin, that same reconstruction but based on the bins used by Serge et. al. (2023) and Zanon et al. (2018). Serge et al. (2023) temporal bins cover 500-year intervals before 700 cal. BP and for 700-350 cal. BP, 350-100 cal. BP and 100 cal. BP- present. Zanon et al. (2018) temporal bins cover 250-year intervals. Although the trend in median tree cover remains the same through time, utilising the longer bin widths from Serge et al. (2023) has the effect of reducing both the variability and the range in median tree cover values.

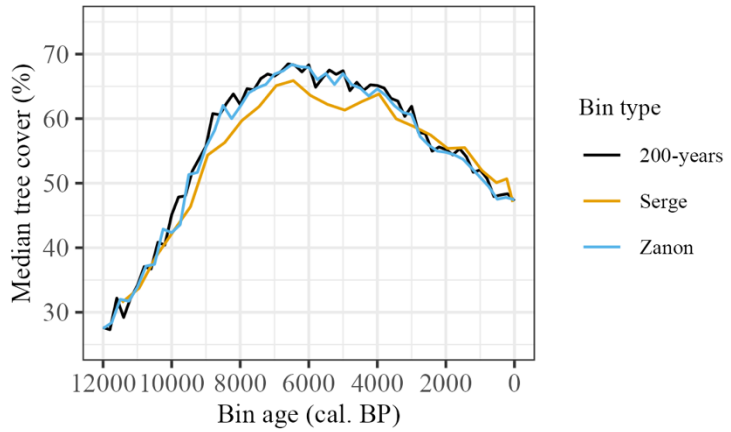

Figure S20: Median reconstructed tree cover for Europe from 12,000 to 0 cal. BP, based on different bin widths used in other vegetation reconstructions.

Section S20: Median reconstructed tree cover on upper and lower age model ranges

There is uncertainty associated with the dates used to construct age-depth models for the pollen records, and this is promulgated into uncertainties assigned to the sample ages in the age model. We investigated the implications of this uncertainty on median tree cover through time, by recalculating median tree cover based on the interquartile ranges of age model values (see Fig. S21). The lower quartile median value represents the 25% lower estimate of ages for each sample (older), with the upper quartile representing the 75% upper estimate of ages (younger). Due to the binning approach however, the impact of using different age model values for each sample is minimal. As Zanon et al. (2018) was published prior to the development of INTCAL20 (Reimer et al., 2020) and Marine20 (Heaton et al., 2020) calibration curves, some differences between our tree cover reconstructions may reflect differences in age models. Similarly, Serge et al. (2023) use the author's original age models, or those published in earlier datasets. Again, this use of different age models may have an impact on the comparison between median tree cover reconstructions.

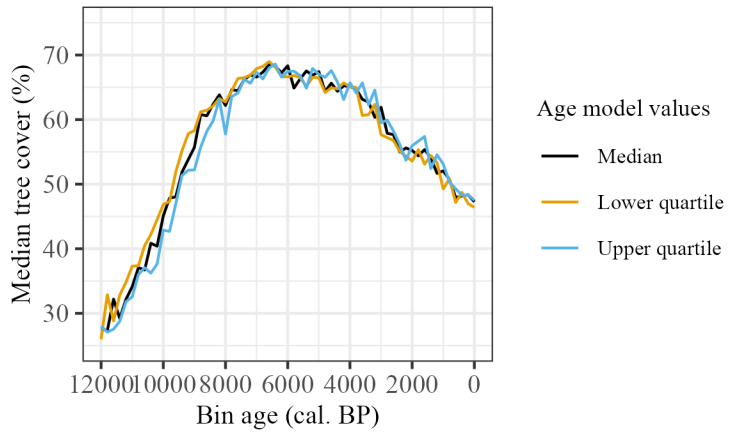

Figure S21: Median reconstructed tree cover for Europe from 12,000 to 0 cal. BP, calculated using different fossil sample age model estimates

Section S21: Median tree cover reconstructions based on grid cell averages

Comparisons of the median tree cover from our reconstructions with those from the Serge et al. (2023) and Zanon et al. (2018) data (Fig. 8) are based on individual pollen record locations. However, as the data from the other reconstructions are grid cell averages, the calculation of the median tree cover through time will include multiple instances of individual grid cells, where record locations share a single grid cell. This is more likely for the Serge et al. (2023) data, where reconstructions are based on larger 1º grid cells. To test the potential implications of multiple fossil record locations being within a single grid cell, Fig. S22 shows median tree cover values for these other reconstructions, but based on single values for each overlapping grid cell. Although the general trend of the tree cover medians remains the same, there is a slight increase in median tree cover values for the median reconstructions based on the data from Serge et al. (2023) and Zanon et al. (2018).

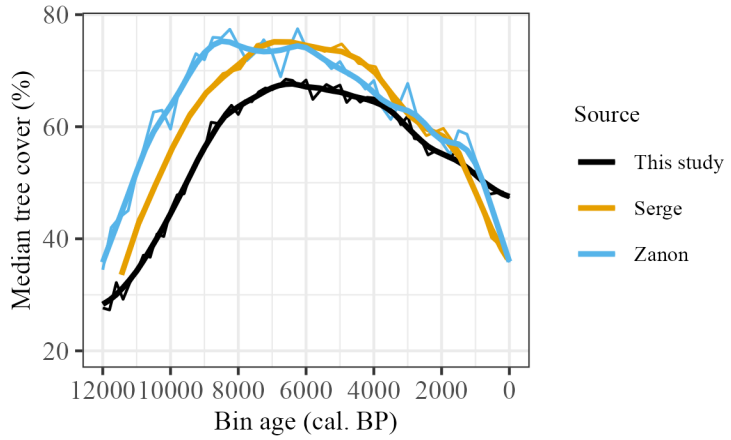

Figure S22: Median reconstructed tree cover for Europe from 12,000 to 0 cal. BP, with reconstructions for Serge et al. (2023) and Zanon et al. (2018) data based on grid cell averages rather than record values. Smoothed lines reflect LOESS fitted regression with 1000-year halfwidth.

Section S22: Median tree cover reconstructions based on the Atlantic, Boreal, Continental and Mediterranean biogeographical regions only

Limiting the data to records within the Atlantic, Boreal, Continental and Mediterranean regions has a limited effect on pan-European median tree cover reconstructions (Fig. S23).

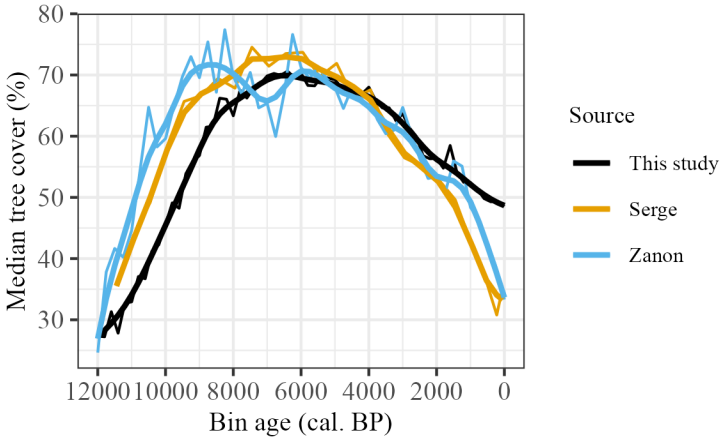

Figure S23: Mean reconstructed tree cover for Europe from 12,000 to 0 cal. BP, based on records within the Atlantic, Boreal, Continental and Mediterranean biogeographical regions only. Smoothed lines reflect LOESS fitted regression with 1000-year halfwidth.

Section S23: Supplementary information references

Adeleye, M. A., Haberle, S. G., McWethy, D., Connor, S. E., and Stevenson, J.: Environmental change during the last glacial on an ancient land bridge of southeast Australia, J Biogeogr, 48, 2946–2960, https://doi.org/10.1111/jbi.14255, 2021a.

Adeleye, M. A., Haberle, S. G., Harris, S., Hopf, F. V., Connor, S., and Stevenson, J.: Holocene heathland development in temperate oceanic Southern Hemisphere: Key drivers in a global context, J Biogeogr, 48, 1048–1062, https://doi.org/10.1111/jbi.14057, 2021b.

Beck, K. K., Fletcher, M.-S., Gadd, P. S., Heijnis, H., and Jacobsen, G. E.: An early onset of ENSO influence in the extra-tropics of the southwest Pacific inferred from a 14, 600 year high resolution multi-proxy record from Paddy's Lake, northwest Tasmania, Quat Sci Rev, 157, 164–175, https://doi.org/10.1016/j.quascirev.2016.12.001, 2017.

Black, M. P., Mooney, S. D., and Haberle, S. G.: The fire, human and climate nexus in the Sydney Basin, eastern Australia, Holocene, 17, 469–480, https://doi.org/10.1177/0959683607077024, 2007.

Bush, M. B., Correa-Metrio, A., van Woesik, R., Collins, A., Hanselman, J., Martinez, P., and McMichael, C. N. H.: Modern pollen assemblages of the Neotropics, J Biogeogr, 48, 231–241, https://doi.org/10.1111/jbi.13960, 2021.

Chen, H.-Y., Xu, D.-Y., Liao, M.-N., Li, K., Ni, J., Cao, X.-Y., Cheng, B., Hao, X.-D., Kong, Z.-C., Li, S.-F., Li, X.-Q., Liu, G.-X., Liu, P.-M., Liu, X.-Q., Sun, X.-J., Tang, L.-Y., Wei, H.-C., Xu, Q.-H., Yan, S., Yang, X.-D., Yang, Z.-J., Yu, G., Zhang, Y., Zhang, Z.-Y., Zhao, K.-L., Zheng, Z., and Ulrike, H.: A modern pollen dataset of China, Chinese Journal of Plant Ecology, 45, 799–808, https://doi.org/10.17521/cjpe.2021.0024, 2021.

Davis, B. A. S., Chevalier, M., Sommer, P., Carter, V. A., Finsinger, W., Mauri, A., Phelps, L. N., Zanon, M., Abegglen, R., Åkesson, C. M., Alba-Sánchez, F., Anderson, R. S., Antipina, T. G., Atanassova, J. R., Beer, R., Belyanina, N. I., Blyakharchuk, T. A., Borisova, O. K., Bozilova, E., Bukreeva, G., Bunting, M. J., Clò, E., Colombaroli, D., Combourieu-Nebout, N., Desprat, S., Di Rita, F., Djamali, M., Edwards, K. J., Fall, P. L., Feurdean, A., Fletcher, W., Florenzano, A., Furlanetto, G., Gaceur, E., Galimov, A. T., Gałka, M., García-Moreiras, I., Giesecke, T., Grindean, R., Guido, M. A., Gvozdeva, I. G., Herzschuh, U., Hjelle, K. L., Ivanov, S., Jahns, S., Jankovska, V., Jiménez-Moreno, G., Karpińska-Kołaczek, M., Kitaba, I., Kołaczek, P., Lapteva, E. G., Latałowa, M., Lebreton, V., Leroy, S., Leydet, M., Lopatina, D. A., López-Sáez, J. A., Lotter, A. F., Magri, D., Marinova, E., Matthias, I., Mavridou, A., Mercuri, A. M., Mesa-Fernández, J. M., Mikishin, Y. A., Milecka, K., Montanari, C., Morales-Molino, C., Mrotzek, A., Muñoz Sobrino, C., Naidina, O. D., Nakagawa, T., Nielsen, A. B., Novenko, E. Y., Panajiotidis, S., Panova, N. K., Papadopoulou, M., Pardoe, H. S., Pędziszewska, A., Petrenko, T. I., Ramos-Román, M. J., Ravazzi, C., Rösch, M., Ryabogina, N., Sabariego Ruiz, S., Salonen, J. S., Sapelko, T. V., Schofield, J. E., Seppä, H., Shumilovskikh, L., Stivrins, N., Stojakowits, P., Svobodova Svitavska, H., Święta-Musznicka, J., Tantau, I., Tinner, W.,

Tobolski, K., Tonkov, S., Tsakiridou, M., et al.: The Eurasian Modern Pollen Database (EMPD), version 2, Earth Syst Sci Data, 12, 2423–2445, https://doi.org/10.5194/essd-12-2423-2020, 2020.
Dodson, J. R.: A vegetation history from north-east Nelson, New Zealand, N Z J Bot, 16, 371–378, https://doi.org/10.1080/0028825X.1978.10425144, 1978.
Dodson, J. R. and Intoh, M.: Prehistory and palaeoecology of Yap, federated states of Micronesia, Quaternary International, 59, 17–26, https://doi.org/10.1016/S1040-6182(98)00068-8, 1999.
Dugerdil, L., Joannin, S., Peyron, O., Jouffroy-Bapicot, I., Vannière, B., Boldgiv, B., Unkelbach, J., Behling, H., and Ménot, G.: Climate reconstructions based on GDGT and pollen surface datasets from Mongolia and Baikal area: calibrations and applicability to extremely cold–dry environments over the Late Holocene, Climate of the Past, 17, 1199–1226, https://doi.org/10.5194/cp-17-1199-2021, 2021.
European Environment Agency: Biogeographical regions, https://sdi.eea.europa.eu/catalogue/srv/api/records/11db8d14-f167-4cd5-9205-95638dfd9618, 2016.
Heaton, T. J., Köhler, P., Butzin, M., Bard, E., Reimer, R. W., Austin, W. E. N., Bronk Ramsey, C., Grootes, P. M., Hughen, K. A., Kromer, B., Reimer, P. J., Adkins, J., Burke, A., Cook, M. S., Olsen, J., and Skinner, L. C.: Marine20—The Marine Radiocarbon Age Calibration Curve (0–55,000 cal BP), Radiocarbon, 62, 779–820, https://doi.org/10.1017/RDC.2020.68, 2020.
Hengl, T., Walsh, M. G., Sanderman, J., Wheeler, I., Harrison, S. P., and Prentice, I. C.: Global mapping of potential natural vegetation: an assessment of machine learning algorithms for estimating land potential, PeerJ, 6, e5457, https://doi.org/10.7717/peerj.5457, 2018.
Field, E., Tyler, J., Gadd, P. S., Moss, P., McGowan, H., and Marx, S.: Coherent patterns of environmental change at multiple organic spring sites in northwest Australia: Evidence of Indonesian-Australian summer monsoon variability over the last 14,500 years, Quat Sci Rev, 196, 193–216, https://doi.org/10.1016/j.quascirev.2018.07.018, 2018.
Fletcher, M.-S., Wood, S. W., and Haberle, S. G.: A fire-driven shift from forest to non-forest: evidence for alternative stable states?, Ecology, 95, 2504–2513, https://doi.org/10.1890/12-1766.1, 2014.
Gaillard, M.-J., Birks, H. J. B., Emanuelsson, U., and Berglund, B. E.: Modern pollen/land-use relationships as an aid in the reconstruction of past land-uses and cultural landscapes: an example from south Sweden, Veg Hist Archaeobot, 1, https://doi.org/10.1007/BF00190697, 1992.
Gudmundsson, L., Bremnes, J. B., Haugen, J. E., and Engen-Skaugen, T.: Technical Note: Downscaling RCM precipitation to the station scale using statistical transformations - a comparison of methods, Hydrol. Earth Syst. Sci., 16, 3383–3390, https://doi.org/10.5194/hess-16-3383-2012, *qmap* version 1.0-6, 2012.
Reimer, P. J., Austin, W. E. N., Bard, E., Bayliss, A., Blackwell, P. G., Bronk Ramsey, C., Butzin, M., Cheng, H., Edwards, R. L., Friedrich, M., Grootes, P. M., Guilderson, T. P., Hajdas, I., Heaton, T. J., Hogg, A. G., Hughen, K. A., Kromer, B., Manning, S. W., Muscheler, R., Palmer, J. G., Pearson, C., van der Plicht, J., Reimer, R. W., Richards, D. A., Scott, E. M., Southon, J. R., Turney, C. S. M., Wacker, L., Adolphi, F., Büntgen, U., Capano, M., Fahrni, S. M., Fogtmann-Schulz, A., Friedrich, R.,

Köhler, P., Kudsk, S., Miyake, F., Olsen, J., Reinig, F., Sakamoto, M., Sookdeo, A., and Talamo, S.: The IntCal20 Northern Hemisphere Radiocarbon Age Calibration Curve (0–55 cal kBP), Radiocarbon, 62, 1–33, https://doi.org/10.1017/rdc.2020.41, 2020.

Haberle, S.: Late quaternary environmental history of the Tari Basin, Papua New Guinea (PhD Thesis), Australian National University, Canberra, 1993.

Haberle, S.: Explanations for palaeoecological changes on the northern plains of Guadalcanal, Solomon Islands: the last 3200 years, Holocene, 6, 333–338, https://doi.org/10.1177/095968369600600307, 1996.

Harrison, S. P.: Modern pollen data for climate reconstructions, version 1 (SMPDS), University of Reading. Dataset, 2019.

Harrison, S. P., Marinova, E., and Cruz-Silva, E.: EMBSeCBIO pollen database, University of Reading. Dataset, 2021.

Harrison, S. P., Shen, Y., and Sweeney, L.: Pollen data and charcoal data of the Iberian Peninsula (version 3), University of Reading. Dataset, 2022a.

Harrison, S. P., Villegas-Diaz, R., Cruz-Silva, E., Gallagher, D., Kesner, D., Lincoln, P., Shen, Y., Sweeney, L., Colombaroli, D., Ali, A., Barhoumi, C., Bergeron, Y., Blyakharchuk, T., Bobek, P., Bradshaw, R., Clear, J. L., Czerwiński, S., Daniau, A.-L., Dodson, J., Edwards, K. J., Edwards, M. E., Feurdean, A., Foster, D., Gajewski, K., Gałka, M., Garneau, M., Giesecke, T., Gil Romera, G., Girardin, M. P., Hoefer, D., Huang, K., Inoue, J., Jamrichová, E., Jasiunas, N., Jiang, W., Jiménez-Moreno, G., Karpińska-Kołaczek, M., Kołaczek, P., Kuosmanen, N., Lamentowicz, M., Lavoie, M., Li, F., Li, J., Lisitsyna, O., López-Sáez, J. A., Luelmo-Lautenschlaeger, R., Magnan, G., Magyari, E. K., Maksims, A., Marcisz, K., Marinova, E., Marlon, J. R., Mensing, S., Miroslaw-Grabowska, J., Oswald, W., Pérez-Díaz, S., Pérez-Obiol, R., Piilo, S., Poska, A., Qin, X., Remy, C. C., Richard, P. J. H., Salonen, S., Sasaki, N., Schneider, H., Shotyk, W., Stancikaite, M., Šteinberga, D., Stivrins, N., Takahara, H., Tan, Z., Trasune, L., Umbanhowar, C. E., Väliranta, M., Vassiljev, J., Xiao, X., Xu, Q., Xu, X., Zawisza, E., Zhao, Y., Zhou, Z., and Paillard, J.: The Reading Palaeofire Database: an expanded global resource to document changes in fire regimes from sedimentary charcoal records, Earth Syst Sci Data, 14, 1109–1124, https://doi.org/10.5194/essd-14-1109-2022, 2022b.

Herzschuh, U., Cao, X., Laepple, T., Dallmeyer, A., Telford, R. J., Ni, J., Chen, F., Kong, Z., Liu, G., Liu, K.-B., Liu, X., Stebich, M., Tang, L., Tian, F., Wang, Y., Wischnewski, J., Xu, Q., Yan, S., Yang, Z., Yu, G., Zhang, Y., Zhao, Y., and Zheng, Z.: Position and orientation of the westerly jet determined Holocene rainfall patterns in China, Nat Commun, 10, 2376, https://doi.org/10.1038/s41467-019-09866-8, 2019.

Hope, G.: Environmental change and fire in the Owen Stanley Ranges, Papua New Guinea, Quat Sci Rev, 28, 2261–2276, https://doi.org/10.1016/j.quascirev.2009.04.012, 2009.

Hope, G., Gillieson, D., and Head, J.: A Comparison of Sedimentation and Environmental Change in New Guinea Shallow Lakes, J Biogeogr, 15, 603, https://doi.org/10.2307/2845439, 1988.

Hope, G., O'Dea, D., and Southern, W.: Holocene vegetation histories in the Western Pacific: alternative records of human impact, in: The Pacific from 5000 to 2000 BP : colonisation and transformations, edited by: Galipaud, J.-C. and Lilley, I., IRD, Paris, 387–404, 1996.

Jolly, D., R. Bonnefille, S. Burcq, and M. Roux. Représentation pollinique de la forêt dense humide du Gabon, tests statistiques. Comptes rendus de l'Académie des sciences. Série II a, Sciences de la terre et des planètes 322(1):63-70, 1996.

Julier, A. C. M., Jardine, P. E., Adu-Bredu, S., Coe, A. L., Duah-Gyamfi, A., Fraser, W. T., Lomax, B. H., Malhi, Y., Moore, S., Owusu-Afriyie, K., and Gosling, W. D.: The modern pollen–vegetation relationships of a tropical forest–savannah mosaic landscape, Ghana, West Africa, Palynology, 42, 324–338, https://doi.org/10.1080/01916122.2017.1356392, 2018.

Julier, A. C. M., Jardine, P. E., Adu-Bredu, S., Coe, A. L., Fraser, W. T., Lomax, B. H., Malhi, Y., Moore, S., and Gosling, W. D.: Variability in modern pollen rain from moist and wet tropical forest plots in Ghana, West Africa, Grana, 58, 45–62, https://doi.org/10.1080/00173134.2018.1510027, 2019.

Kling, M. M. and Ackerly, D. D.: Global wind patterns shape genetic differentiation, asymmetric gene flow, and genetic diversity in trees, Proceedings of the National Academy of Sciences, 118, https://doi.org/10.1073/pnas.2017317118, 2021.

Lebamba, J., Vincens, A., Jolly, D., Ngomanda, A., Schevin, P., Maley, J., and Bentaleb, I.: Modern pollen rain in savanna and forest ecosystems of Gabon and Cameroon, Central Atlantic Africa, Rev Palaeobot Palynol, 153, 34–45, https://doi.org/10.1016/j.revpalbo.2008.06.004, 2009.

Luly, J. G.: Holocene Palaeoenvironments Near Lake Tyrrell, Semi-Arid Northwestern Victoria, Australia, J Biogeogr, 20, 587, https://doi.org/10.2307/2845516, 1993.

Luly, J. G., Bowler, J. M., and Head, M. J.: A radiocarbon chronology from the playa Lake Tyrrell, Northwestern Victoria, Australia, Palaeogeogr Palaeoclimatol Palaeoecol, 54, 171–180, https://doi.org/10.1016/0031-0182(86)90123-9, 1986.

Macphail, M. K.: The history of the vegetation and climate in southern Tasmania since the late Pleistocene (ca. 13. 000 - 0 BP)(Doctoral Dissertation), University of Tasmania, 1975.

Macphail, M. K.: Vegetation and Climates in Southern Tasmania since the Last Glaciation, Quat Res, 11, 306–341, https://doi.org/10.1016/0033-5894(79)90078-4, 1979.

Macphail, M. K.: Fossil and modern *Beilschmiedia* (lauraceae) pollen in New Zealand, N Z J Bot, 18, 453–457, https://doi.org/10.1080/0028825X.1980.10425165, 1980.

Macphail, M. K. and McQueen, D. R.: The value of New Zealand pollen and spores as indicators of Cenozoic vegetation and climates, Tuatara, 26, 37–56, 1983.

Macphail, M. K. and Mildenhall, D. C.: *Dactylanthus taylori:* in North-West Nelson, New Zealand?, N Z J Bot, 18, 149–152, https://doi.org/10.1080/0028825X.1980.10427242, 1980.

Mariani, M., Connor, S. E., Fletcher, M., Theuerkauf, M., Kuneš, P., Jacobsen, G., Saunders, K. M., and Zawadzki, A.: How old is the Tasmanian cultural landscape? A test of landscape openness using

quantitative land-cover reconstructions, J Biogeogr, 44, 2410–2420, https://doi.org/10.1111/jbi.13040, 2017.

McWethy, D. B., Whitlock, C., Wilmshurst, J. M., McGlone, M. S., Fromont, M., Li, X., Dieffenbacher-Krall, A., Hobbs, W. O., Fritz, S. C., and Cook, E. R.: Rapid landscape transformation in South Island, New Zealand, following initial Polynesian settlement, Proceedings of the National Academy of Sciences, 107, 21343–21348, https://doi.org/10.1073/pnas.1011801107, 2010.

McWethy, D. B., Wilmshurst, J. M., Whitlock, C., Wood, J. R., and McGlone, M. S.: A High-Resolution Chronology of Rapid Forest Transitions following Polynesian Arrival in New Zealand, PLoS One, 9, e111328, https://doi.org/10.1371/journal.pone.0111328, 2014.

Norton, D. A., McGlone, M. S., and Wigley, T. M. L.: Quantitative analyses of modern pollen-climate relationships in New Zealand indigenous forests, N Z J Bot, 24, 331–342, https://doi.org/10.1080/0028825X.1986.10412681, 1986.

Phelps, L. N., Chevalier, M., Shanahan, T. M., Aleman, J. C., Courtney-Mustaphi, C., Kiahtipes, C. A., Broennimann, O., Marchant, R., Shekeine, J., Quick, L. J., Davis, B. A. S., Guisan, A., and Manning, K.: Asymmetric response of forest and grassy biomes to climate variability across the African Humid Period: influenced by anthropogenic disturbance?, Ecography, 43, 1118–1142, https://doi.org/10.1111/ecog.04990, 2020.

Pickett, E. J., Harrison, S. P., Hope, G., Harle, K., Dodson, J. R., Peter Kershaw, A., Colin Prentice, I., Backhouse, J., Colhoun, E. A., D'Costa, D., Flenley, J., Grindrod, J., Haberle, S., Hassell, C., Kenyon, C., Macphail, M., Martin, H., Martin, A. H., McKenzie, M., Newsome, J. C., Penny, D., Powell, J., Ian Raine, J., Southern, W., Stevenson, J., Sutra, J., Thomas, I., van der Kaars, S., and Ward, J.: Pollen-based reconstructions of biome distributions for Australia, Southeast Asia and the Pacific (SEAPAC region) at 0, 6000 and 18,000 ^{14} C yr BP, J Biogeogr, 31, 1381–1444, https://doi.org/10.1111/j.1365-2699.2004.01001.x, 2004.

Prebble, M., Kennedy, J., and Southern, W.: Holocene lowland vegetation change and human ecology in Manus Province, Papua New Guinea, in: Altered Ecologies (Terra Australis 32): Fire, climate and human influence on terrestrial landscapes, ANU Press, https://doi.org/10.22459/TA32.11.2010.12, 2010.

Prebble, M., Anderson, A. J., Augustinus, P., Emmitt, J., Fallon, S. J., Furey, L. L., Holdaway, S. J., Jorgensen, A., Ladefoged, T. N., Matthews, P. J., Meyer, J.-Y., Phillipps, R., Wallace, R., and Porch, N.: Early tropical crop production in marginal subtropical and temperate Polynesia, Proceedings of the National Academy of Sciences, 116, 8824–8833, https://doi.org/10.1073/pnas.1821732116, 2019.

Serge, M., Mazier, F., Fyfe, R., Gaillard, M.-J., Klein, T., Lagnoux, A., Galop, D., Githumbi, E., Mindrescu, M., Nielsen, A., Trondman, A.-K., Poska, A., Sugita, S., Woodbridge, J., Abel-Schaad, D., Åkesson, C., Alenius, T., Ammann, B., Andersen, S., Anderson, R., Andrič, M., Balakauskas, L., Barnekow, L., Batalova, V., Bergman, J., Birks, H., Björkman, L., Bjune, A., Borisova, O., Broothaerts, N., Carrion, J., Caseldine, C., Christiansen, J., Cui, Q., Currás, A., Czerwiński, S., David, R., Davies,

A., De Jong, R., Di Rita, F., Dietre, B., Dörfler, W., Doyen, E., Edwards, K., Ejarque, A., Endtmann, E., Etienne, D., Faure, E., Feeser, I., Feurdean, A., Fischer, E., Fletcher, W., Franco-Múgica, F., Fredh, E., Froyd, C., Garcés-Pastor, S., García-Moreiras, I., Gauthier, E., Gil-Romera, G., González-Sampériz, P., Grant, M., Grindean, R., Haas, J., Hannon, G., Heather, A.-J., Heikkilä, M., Hjelle, K., Jahns, S., Jasiunas, N., Jiménez-Moreno, G., Jouffroy-Bapicot, I., Kabailienė, M., Kamerling, I., Kangur, M., Karpińska-Kołaczek, M., Kasianova, A., Kołaczek, P., Lagerås, P., Latalowa, M., Lechterbeck, J., Leroyer, C., Leydet, M., Lindbladh, M., Lisitsyna, O., López-Sáez, J.-A., Lowe, J., Luelmo-Lautenschlaeger, R., Lukanina, E., Macijauskaitė, L., Magri, D., Marguerie, D., Marquer, L., Martinez-Cortizas, A., Mehl, I., Mesa-Fernández, J., Mighall, T., Miola, A., Miras, Y., Morales-Molino, C., et al.: Testing the Effect of Relative Pollen Productivity on the REVEALS Model: A Validated Reconstruction of Europe-Wide Holocene Vegetation, Land (Basel), 12, 986, https://doi.org/10.3390/land12050986, 2023.

Shulmeister, J., McLea, W. L., Singer, C., McKay, R. M., and Hosie, C.: Late Quaternary pollen records from the Lower Cobb Valley and adjacent areas, North-West Nelson, New Zealand, N Z J Bot, 41, 503–533, https://doi.org/10.1080/0028825X.2003.9512867, 2003.

Takahara, H., Sugita, S., Harrison, S. P., Miyoshi, N., Morita, Y., and Uchiyama, T.: Pollen-based reconstructions of Japanese biomes at 0, 6000 and 18,000 ^{14}C yr <scp>bp</scp>, J Biogeogr, 27, 665–683, https://doi.org/10.1046/j.1365-2699.2000.00432.x, 2000.

Tong, Z.-Y., Wu, L.-Y., Feng, H.-H., Zhang, M., Armbruster, W. S., Renner, S. S., and Huang, S.-Q.: New calculations indicate that 90% of flowering plant species are animal-pollinated, Natl Sci Rev, 10, https://doi.org/10.1093/nsr/nwad219, 2023.

Villegas-Diaz, R. and Harrison, S. P.: smpds: The SPECIAL Modern Pollen Data Set for Climate Reconstructions. Software. 2022.

Vincens, A., Lézine, A.-M., Buchet, G., Lewden, D., and Le Thomas, A.: African pollen database inventory of tree and shrub pollen types, Rev Palaeobot Palynol, 145, 135–141, https://doi.org/10.1016/j.revpalbo.2006.09.004, 2007.

Williams, J. W., Grimm, E. C., Blois, J. L., Charles, D. F., Davis, E. B., Goring, S. J., Graham, R. W., Smith, A. J., Anderson, M., Arroyo-Cabrales, J., Ashworth, A. C., Betancourt, J. L., Bills, B. W., Booth, R. K., Buckland, P. I., Curry, B. B., Giesecke, T., Jackson, S. T., Latorre, C., Nichols, J., Purdum, T., Roth, R. E., Stryker, M., and Takahara, H.: The Neotoma Paleoecology Database, a multiproxy, international, community-curated data resource, Quat Res, 89, 156–177, https://doi.org/10.1017/qua.2017.105, 2018.

Zanon, M., Davis, B. A. S., Marquer, L., Brewer, S., and Kaplan, J. O.: European forest cover during the past 12,000 years: A palynological reconstruction based on modern analogs and remote sensing, Front. Plant Sci., 9, 1–25, https://doi.org/10.3389/fpls.2018.00253, 2018.